

# Models of liquid samples confinement for nanoscale NMR

Santiago Oviedo-Casado,<sup>1,\*</sup> Daniel Cohen,<sup>2,†</sup> and Javier Cerrillo<sup>1,‡</sup>

<sup>1</sup>*Área de Física Aplicada, Universidad Politécnica de Cartagena, Cartagena E-30202, Spain*

<sup>2</sup>*Racah Institute of Physics, Hebrew University of Jerusalem, 91904 Jerusalem, Israel*

Diffusion is a prominent source of noise affecting nuclear magnetic resonance at the nanometer scale (nano-NMR), preventing high resolution studies of unpolarized liquid samples. Actively managing diffusion noise through, for example, sample confinement, is likely to unveil alternative noise sources which so far have been disregarded, as they occur in longer time-scales and are, consequently, masked by diffusion. These secondary noise sources could diminish the advantages provided by sample confinement but, on the other hand, they can provide with valuable information about the behavior of the sample and its interactions. In this article, we study for the first time and in detail two noise models for confined nano-NMR, namely, surface interactions and porosity, and discuss their implications for typical nano-NMR experiments.

## I. INTRODUCTION

Nuclear magnetic resonance (NMR) spectroscopy is a fundamental tool to study molecular structures and sample composition. Based on detecting the magnetic field produced by the precessing spin of specific atomic nuclei in molecules, NMR is widely employed to chemically analyze samples of relevance in fields ranging from material sciences to pharmacology. Despite having driven fundamental scientific breakthroughs in the last decades, it is an accepted truth that NMR is limited by a low sensitivity that demands substantial amounts of sample to achieve the desired precision for sample characterization [1]. Various solutions are currently being explored to improve the sensitivity of NMR while at the same time reducing the sample size, for example micro-coils [2, 3]. Among them, quantum sensors offer a most promising route [4].

Quantum sensors have demonstrated a remarkable ability to outperform their classical counterparts [5]. Using definite quantum properties permits estimating physical parameters with a precision far beyond what is achievable in the classical limit [6]. One of the best developed quantum sensing technologies is the NMR analogue, which consists of a controllable spin that can be brought in close contact with the sample, thereby allowing to reduce the sample size at minimal expense in sensitivity. The most prominent platform for quantum sensing NMR is the nitrogen vacancy (NV) center in diamond [7], which has been shown to be capable of detecting the magnetic field produced by the nuclei in nano-sized samples of molecules at ambient conditions [8–15]. At these scales, where the detector lies at a distance of only a few nm from the sample, the statistical polarization dominates over the thermal averaging [16–18], allowing to perform room-temperature nanoscale NMR (nano-NMR) in pristine samples.

Despite the practical advantages that they offer, quantum sensors feature their own set of limitations, the main ones being: The noise affecting the quantum properties of the sensor, the noise affecting the coupling between the sensor and the sample, and the backaction that the sensor induces on the sample. The first kind can be substantially mitigated using techniques such as dynamical decoupling [19–21], while backaction can be utilized, in some scenarios, to increase precision [22]. Coupling noise, however, which in NMR experiments is typically dominated by diffusion of the molecules in the liquid state sample, is harder to manage without actively manipulating the sample, forfeiting the intended result for which nano-NMR was designed.

The problem of coupling noise stems from the dipole-dipole interaction which is the main coupling between the nuclei in the sample and spin sensor in nano-NMR. The dipole-dipole coupling is strongly distance-dependent, resulting in a detected signal to which only the closest nuclei contribute significantly. Diffusion yields a characteristic time-scale for the statistically polarized nuclei to become, on average, too distant from the sensor to generate a signal of amplitude larger than the background noise, at which point no meaningful information can be gained from the sample. Thus, diffusion limits the precision with which the sample can be studied. On the other hand, the random nature of diffusion transfers to the couplings between nuclei and sensor, which fluctuate accordingly. Using noise spectroscopy techniques allows us to elucidate the nature of these fluctuations and, in that way, study the underlying diffusion model [23, 24]. We propose that this knowledge can in principle be utilized to identify physical processes occurring in the sample, manage the impact of diffusion in spectroscopy, and lead to increased precision.

---

\* [santiago.oviedo@upct.es](mailto:santiago.oviedo@upct.es)

† [daniel.cohen7@mail.huji.ac.il](mailto:daniel.cohen7@mail.huji.ac.il)

‡ [javier.cerrillo@upct.es](mailto:javier.cerrillo@upct.es)

A possible route to eliminate the problem of diffusion noise is to confine the sample to an enclosed volume of size comparable to that of the sensing region [25, 26]. In the confined model, nuclei, rather than simply diffusing away from the sensor, remain, on average, within a distance defined by the size of the confining volume, resulting in an ideal steady state in which the signal is no longer affected by diffusion, and from which important properties of the sample can be estimated with increased precision. This model, however, disregards other noise sources whose time-scale is longer than that of diffusion, which become dominant once diffusion is mitigated. Among these, we find nuclei relaxation [27], or surface interactions [28, 29], all of which means that, ultimately, spectroscopic sensitivity is limited, but also that valuable information about the behavior of the sample components can be extracted by comparing with the appropriate noise models.

In this article, we tackle the problem of understanding realistic confinement in a nano-NMR setting, with noise sources other than diffusion affecting the ability to extract information from the sample. To do so, we solve analytically the diffusion equation on a confined region of the space, in which we conceptualize two different mechanisms of signal decay rather than diffusion, which for clarity we consider separately. In the first case, we model the nuclei transitioning from a confining volume to a confining (trapping) surface at a rate dictated by diffusion. We name this mechanism *sticky walls*, as it describes the nuclei being immobilized upon arrival at the confining volume walls, as illustrated in Fig. 1a), effectively reducing the diffusion coefficient to zero due to, for example, a mild electromagnetic interaction. For the second scenario, we consider a confining volume from which nuclei evaporate (dissipate) at a given, fixed rate. With this model, which we call *evaporating walls*, we aim to describe, through a heuristic model, orientation changes in the nuclei due to interaction with the walls or porous confining volumes, as shown in Fig. 1a), that lead to a randomization of the interactions and, thereby, the decay of the statistical polarization.

With the proposed models, we shed a first light onto various different noise processes occurring on nano-sized confined fluids, and the way they get imprinted as different regimes in the detected signal, which in this setting corresponds to the autocorrelation of the magnetic field created by the statistically polarized nuclei at the probe's position, as displayed in Fig. 1b), which then can be used to infer important properties about the sample and its interactions with the quantum sensor environment. The information provided by the specific shape of the autocorrelation, together with the theoretical analysis that we present, can then be taken advantage of to decide the optimal experimental parameters and to improve the experiment design. As well, we demonstrate how the confinement regime can lead to enhanced parameter estimation in NMR spectroscopy. Moreover, our analysis provides realistic scenarios with which to compare whether indeed confining a sample is a reasonable strategy in terms of spectroscopic precision, for different regimes.

The article is organized as follows: first, we describe our imagined setting for confined nano-NMR, and explain the procedure to calculate the correlation functions, which we then explicitly derive for the different noise mechanisms considered, providing the necessary mathematical details for their calculation. Afterwards, we numerically study the behavior of the correlations for different confinement volumes and noise models settings, and analytically derive simple expressions to understand the physics of said behavior. Finally, we demonstrate the capabilities of a confined sample in terms of spectral resolution.

## II. METHODOLOGY

Our aim is to understand the properties and behavior of a confined distribution of molecules, through the interaction of certain nuclei in the molecules with an electronic spin. The setting is a shallow NV center in a diamond, namely, an NV center that is located at a depth  $d$  of a few nm below the diamond surface and, consequently, in close contact with the sample sitting in that surface. We conceive that the confining volume has a cylindrical geometry of volume  $V$ , with the NV center aligned with the  $z$  symmetry axis of the cylinder, as shown in Fig. 1a).

The NV center can be treated as a spin-1/2 two-level system ( $\vec{S}$ ) that interacts with a nucleus ( $\vec{I}$ ) in the sample through the dipole-dipole Hamiltonian

$$\frac{H_{DD}}{\gamma_e \Upsilon} = \frac{3(\vec{S} \cdot \hat{r})(\vec{I} \cdot \hat{r}) - \vec{S} \cdot \vec{I}}{|r|^3}, \quad (1)$$

where  $\gamma_e$  is the gyromagnetic ratio of the electron and  $\Upsilon = \hbar\mu_0\gamma_N/4\pi$ , with  $\gamma_N$  the gyromagnetic ratio of the nuclei.  $\vec{r}$  is the distance between the NV center and each nuclei and the Hamiltonian is given in units of frequency. The  $|r|^{-3}$  dependence defines the characteristics of the interaction, as distant nuclei hardly contribute to the overall detected signal, which corresponds to the time evolution of an initial superposition state of the NV center interacting with the nuclei in the sample. Then, a measurement of the NV center state at a given time reflects an instantaneous realization of the magnetic field that is produced by the statistically polarized nuclei, which we model as  $B(t) = \sum_i a_i(t) \cos(\omega_i t) + b_i(t) \sin(\omega_i t)$ , where the amplitudes  $\{a_i(t), b_i(t)\}$  fluctuate according to the noise affecting the

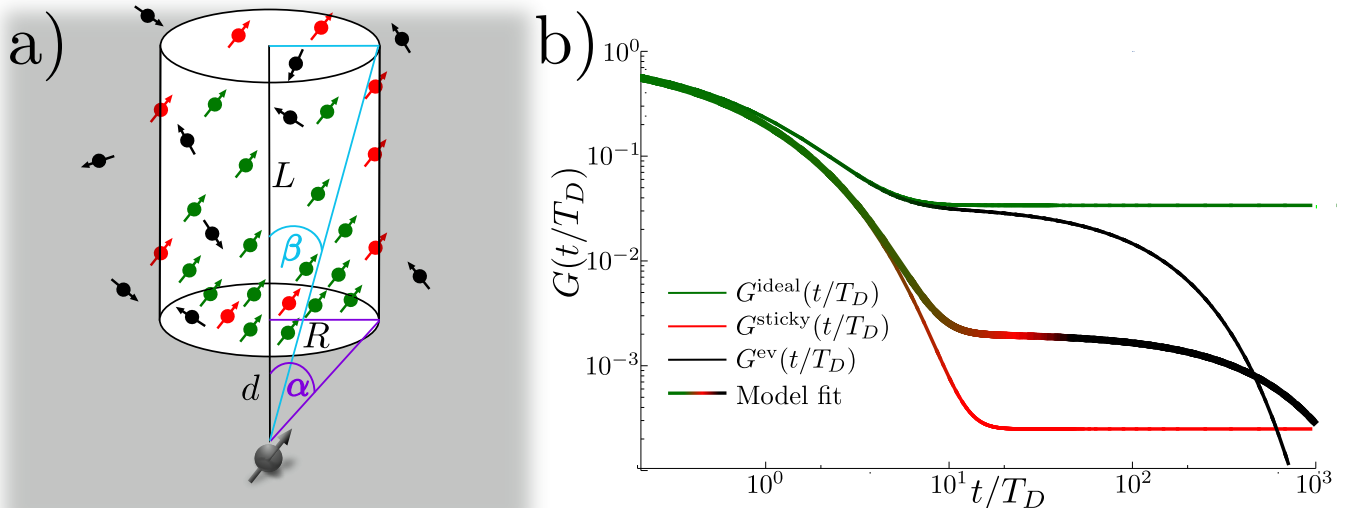


Figure 1. a) Schematic depiction of the considered setup, with a cylinder volume of radius  $R$  and height  $L$  carved on the surface of a diamond that encloses it on all sides. Inside this volume the nuclei in the sample diffuse freely. The diamond matrix features an atomic defect located at a depth  $d$  below the cylinder lower cap, aligned with the symmetry axis of the cylinder. The defect position spans an angle  $\alpha$  with respect to the lower border of the cylinder and an angle  $\beta$  with respect to the upper border. The nuclei in the sample get statistically polarized (green) and diffuse through the confinement volume. Upon touching the walls, we consider three different conceptual model scenarios: the nuclei can rebound unchanged (green), they remain attached to the surface without changing their orientation (red), alter their orientation such that they no longer contribute to the polarization signal (black), or evaporate from the confinement region (black). Each of these scenarios induces a distinct magnetic field at the NV position. (b) Logarithmic scale time dependence of the correlation function for the magnetic field at the NV position for each of the noise models considered, which represents the post-processed signal that is analyzed following an experiment. Nuclei that rebound unchanged keep contributing to the overall correlations, which after some initial decay due to diffusion, then reaches a *plateau* (green) in which diffusion is, effectively, stalled. Nuclei that get stuck to the walls keep contributing to the overall signal, albeit yielding a generally smaller *plateau* amplitude (red), owing to being, on average, more distant from the sensor. Nuclei that lose their orientation or seep out of the confinement volume produce a decrease of the correlation signal (black). The overall behavior of the signal correlation function is likely to be a combination of these models, as shown by the thick, multicolored line, which corresponds to a simple model for the correlations, described in Eq. (28), that includes all the behaviors discussed in this article.

sample, and  $\omega_i$  are the frequencies at which the nuclei precess. For fast diffusing samples, noisy fluctuations change the amplitudes faster than the time it takes to perform a measurement, so to appropriately study the sample the optimal procedure is to target the autocorrelation of the magnetic field  $\langle B(t_0)B(t_0 + t) \rangle$  [30].

The different dipole-dipole interaction components can be resolved by appropriately tuning the external offset magnetic field applied to the NV center probe, such that only one of them dominates the spectrum. Since all of them produce similar results in terms of NV center spin state evolution [31], and yield similar information about the sample, in this article we focus on the  $zz$  component, or flip-flop term. Then, the autocorrelation function corresponding to an initial superposition state of the NV center, evolving under the influence of the magnetic field created by a statistically polarized distribution of diffusing nuclei, is:

$$G(t) = \langle B(t)B(0) \rangle \propto \int \int f(\vec{r})f(\vec{r}_0)P(\vec{r}, t|\vec{r}_0, t=0)d^3rd^3r_0, \quad (2)$$

where  $f(\vec{r}) \propto Y_2^0/|\vec{r}|^3$  represents the form factor for the corresponding dipole-dipole coupling term,  $Y_2^0$  being the spherical harmonic.  $P(\vec{r}, t|\vec{r}_0, t=0)$  is the propagator for the nuclei, which describes the probability of finding a given nucleus at the position  $\vec{r}$  at time  $t$  provided an initial position  $\vec{r}_0$  at the initial time, that we denote as  $t=0$ . The initial distribution of the nuclei is considered to be uniform  $P(\vec{r}_0, t=0) = \text{const}$  over the confining volume. Our first task is then to obtain an expression for  $P(\vec{r}, t|\vec{r}_0, t=0)$ , given diffusion in a finite, confining volume.

In this article, we consider Fickian diffusion [32]. Then, the equation governing the propagator  $P(\vec{r}, t|\vec{r}_0, t=0)$  reads

$$\frac{\partial P}{\partial t} = D\nabla^2 P, \quad (3)$$

where we assume a constant diffusion coefficient  $D$ . In this article, we choose two different sets of boundary conditions to solve Eq. (3), each of them corresponding to a toy model describing a different physical configuration of confined diffusion that yields a particular, characteristic correlation function, and compare each of them to the ideal model of perfectly reflective walls [25].

### III. MATHEMATICAL DERIVATIONS

This section describes the different confined toy models and sketches the mathematical calculations that lead to the correlation functions for each of them, highlighting the relevant equations necessary to understand the results that follow. The full mathematical details can be found in the Appendixes A and B. In all cases, our starting point is the Fickian fluid diffusion equation for the propagator Eq. (3).

#### A. Sticky walls

In this model, we consider that, upon interaction with the walls, the molecules in the sample get attached to the surface of the confinement volume, such that the initial uniform distribution of molecules over the volume ends up distributed over the surface, from where the nuclei keep contributing to the overall statistical polarization, as shown in Fig. 1. The sticky walls model reproduces an extreme case of stick-drag or space dependent diffusion models [33–36], and it is justified by studies suggesting that, near surfaces, fluids tend to staticity [37], experiencing an abrupt transition from the diffusion dynamics happening in the bulk.

We want to calculate the correlation function behavior as the molecules diffuse through the bulk of the confinement volume and become attached to its walls. The propagator in this scenario is a Gaussian that describes free diffusion in the three-dimensional space,

$$P(\vec{r}, t | \vec{r}_0, t = 0) = \frac{1}{(4\pi Dt)^{\frac{3}{2}}} \exp \left[ -\frac{(\vec{r} - \vec{r}_0)^2}{4Dt} \right]. \quad (4)$$

Additionally, we impose the following initial conditions:  $P(\vec{r}, t = 0 | \vec{r}_0, t = 0) = \delta(\vec{r} - \vec{r}_0)$ , where  $\vec{r}_0$  is restricted to  $\rho, \rho_0 \in \{0, R\}$  and  $z, z_0 \in \{d, d + L\}$ , namely, the molecules start off uniformly distributed on the interior of the cylinder.

We are interested in the time evolution of the correlation function. Molecules diffuse in the bulk – the region inside the confining volume – and as they touch the walls, they adhere to that end position and continue contributing to the correlation function. Then, at times much longer than the so-called *volume time*  $-\tau_V \sim \frac{V^{2/3}}{D}$  – that marks the transition from a diffusive regime to a confined regime [25], we can assume that all molecules are distributed on the surface, and we can calculate the asymptotic value of the correlation function exactly as

$$G^{\text{sticky}}(t \gg \tau_V) = \frac{4\pi^2 \Upsilon^2 \zeta}{S} \int_0^R d\rho_0 \rho_0 \int_d^{d+L} dz_0 \frac{Y_2^0(\rho_0, z_0)}{(\rho_0^2 + z_0^2)^{3/2}} \left\{ \int_0^R d\rho \rho \frac{Y_2^0(\rho, d)}{(\rho^2 + d^2)^{3/2}} + \int_0^R d\rho \rho \frac{Y_2^0(\rho, d+L)}{[\rho^2 + (d+L)^2]^{3/2}} + \int_d^{d+L} dz R \frac{Y_2^0(R, z)}{(R^2 + z^2)^{3/2}} \right\}, \quad (5)$$

where  $S$  is the cylinder surface and  $\zeta$  is the nuclear density, which henceforth, for simplicity, we take as  $\zeta = 1$  and omit it.

To calculate the transition period of diffusing molecules we separate the integral in Eq. (2) to two distinct regions. The first one accounts for the molecules diffusing in the bulk, inside the confinement volume. The contribution to the overall correlation of this region is calculated as (see Appendix A for details)

$$G_{\text{bulk}}^{\text{sticky}}(t) = \frac{\sqrt{\pi} \Upsilon^2}{2(Dt)^{\frac{3}{2}}} \int_0^R d\rho \int_0^R d\rho_0 \int_d^{d+L} dz \int_d^{d+L} dz_0 \rho \rho_0 I_0 \left( \frac{\rho \rho_0}{2Dt} \right) \left[ \frac{3z^2}{(\rho^2 + z^2)^{5/2}} - \frac{1}{(\rho^2 + z^2)^{3/2}} \right] \left[ \frac{3z_0^2}{(\rho_0^2 + z_0^2)^{5/2}} - \frac{1}{(\rho_0^2 + z_0^2)^{3/2}} \right] \exp \left( \frac{-\rho^2 - \rho_0^2}{4Dt} \right) \exp \left[ -\frac{(z - z_0)^2}{4Dt} \right]. \quad (6)$$

The second integral aims to measure the contribution from the nuclei that have already reached the walls and have a fixed position there. Considering that all the molecules start inside the cylinder, the contribution from the walls is initially zero, and grows as molecules diffuse out of the confining region. Rather than calculating the population

of nuclei outside the cylinder, and map it to the walls, we can use the conservation of particles and calculate the remaining particles density inside the confining region, which is the integral of the propagator and reads

$$\zeta_{\text{bulk}}^{\text{sticky}}(t) = \frac{\sqrt{\pi}}{2V(Dt)^{\frac{3}{2}}} \int_0^R d\rho \int_0^R d\rho_0 \int_d^{d+L} dz \int_d^{d+L} dz_0 \rho \rho_0 I_0\left(\frac{\rho \rho_0}{2Dt}\right) \exp\left(\frac{-\rho^2 - \rho_0^2}{4Dt}\right) \exp\left[-\frac{(z - z_0)^2}{4Dt}\right], \quad (7)$$

where we use units of the normalized density  $\zeta = 1$  and divide by the confinement region volume  $V$ . Then, the nuclei density on the walls is simply  $1 - \zeta_{\text{bulk}}^{\text{sticky}}(t)$ , and the contribution that they make to the overall correlation function can be calculated from the asymptotic result at long times as  $G_{\text{walls}}^{\text{sticky}}(t) = G^{\text{sticky}}(t \gg \tau_V)[1 - \zeta_{\text{bulk}}^{\text{sticky}}(t)]$ .

Note that both regions need to be calculated numerically. The total correlation function in this sticky walls model is

$$G^{\text{sticky}}(t) = G_{\text{bulk}}^{\text{sticky}}(t) + G_{\text{walls}}^{\text{sticky}}(t). \quad (8)$$

## B. Dissipating walls

The previous model assumes that upon reaching the walls, the nuclei keep their orientation, yielding a finite statistical polarization even at long times. With the second model that we consider now, we aim to describe a polarization decay induced by the confining volume walls. In this model, either the nuclei either rebound from the walls and are dispersed in random directions [38], thereby changing their orientation, or the walls are porous and nuclei slowly seep out of the confining volume [26]. In both cases the result is a decrease in the number of aligned nuclei and, consequently, a weakening of the statistical polarization, as schematically shown in Fig. 1. We describe this scenario with the diffusion equation in confined cylindrical volume with evaporation boundary conditions [39]. Specifically, when solving the differential equation, we allow nuclei to leave the confining volume at a constant rate  $\tau_{\text{ev}}$ , distinct from the diffusion time.

Let us begin by calculating the diffusion propagator in Eq. (3), which in cylindrical coordinates reads

$$\frac{\partial P}{\partial t} - D \left[ \frac{1}{\rho} \frac{\partial}{\partial \rho} \left( \rho \frac{\partial P}{\partial \rho} \right) + \frac{1}{\rho^2} \frac{\partial^2 P}{\partial \phi^2} + \frac{\partial^2 P}{\partial z^2} \right] = 0. \quad (9)$$

The initial distribution of nuclei is the same as in the sticky scenario, the Robin boundary conditions for the radial ( $\rho$ ) and vertical ( $z$ ) coordinates are

$$\left( \frac{\partial P}{\partial \rho} + \frac{d}{D\tau_{\text{ev}}} P \right) \Big|_{\rho=R} = 0, \quad \left( \frac{\partial P}{\partial z} - \frac{d}{D\tau_{\text{ev}}} P \right) \Big|_{z=d} = 0, \quad \left( \frac{\partial P}{\partial z} + \frac{d}{D\tau_{\text{ev}}} P \right) \Big|_{z=d+L} = 0, \quad (10)$$

and the periodic boundary condition on the angular ( $\phi$ ) coordinate is  $P(\phi + 2\pi) = P(\phi)$ . These boundary conditions link the concentration of fluid on both sides of the boundary, with a net flow rate in the direction of lowest concentration. Since we want to consider a confined sample, we assume that the concentration outside of the cylinder (i.e. at infinity) is zero, resulting in a net flow outwards at the defined rate  $\tau_{\text{ev}}^{-1}$ , thus taking into account that, at later times, less nuclei remain in the sample and, as a consequence, evaporation slows down.

We aim to find a solution to Eq (9) using the method of separation of variables. Then

$$P(\vec{r}, t) = T(t)R(\rho)Z(z)e^{-in\phi}, \quad (11)$$

where the angular part is chosen to satisfy the corresponding boundary condition, meaning that  $n \in \mathbb{Z}$ .

As molecules will be evaporating through the surfaces of the confining volume, the concentration in the bulk must be a decreasing function of time. Therefore, the temporal part of the solution must be composed of decaying modes. Thus, we have that

$$T(t) \propto \exp(-D\lambda^2 t), \quad (12)$$

with the eigenvalues  $\lambda \in \mathbb{R}$ . The constant case  $\lambda = 0$  only leads to a trivial solution given the boundary conditions. Consequently, we disregard it.

In the  $z$  dimension, we have a problem defined by the differential equation of the harmonic oscillator kind, which, given the symmetry of the cylinder with respect to its centre, admits solutions in terms of either trigonometric functions or hyperbolic functions. The later however, result in oscillating modes that diverge with time, and so cannot be a solution of a diffusion problem in which the concentration diminishes with time. Then,

$$Z(z) = A_m^- \sin \left[ \eta_m^- \left( z - d - \frac{L}{2} \right) \right] + A_m^+ \sin \left[ \eta_m^+ \left( z - d - \frac{L}{2} \right) \right], \quad (13)$$

where the eigenvalues  $\eta_m^\pm \in \mathbb{R}$  are the discrete solutions to the transcendental equation

$$\left(\frac{\eta_0}{\eta^\pm}\right)^{\pm 1} = \pm \tan \frac{\eta^\pm L}{2}, \quad (14)$$

with  $\eta_0 = d/D\tau_{\text{ev}}$ . The case  $\eta = 0$  does not yield a solution that satisfies the boundary conditions.

This leaves us with the radial and angular parts. The radial part is analogous to the modes featured by an oscillating two-dimensional membrane, admitting solutions in terms of Bessel functions, which must be symmetric with respect to the central axis of the cylinder. Since regularity is required at zero radius (i.e. at the central axis of the cylinder), the only possible solution is  $R(\rho) \propto J_n(\beta\rho)$ , which means that for every eigenvalue  $n$  of the angular component, there is a Bessel solution in the radial dimension. Given the boundary condition, the eigenvalues  $\beta$  are strictly positive, and can be calculated as the solutions to the equation

$$J'_n(\xi) + \frac{dR}{\xi D\tau_{\text{ev}}} J_n(\xi) = 0, \quad \xi = \beta R. \quad (15)$$

Then, for each  $n$ , there is a family  $p = 0, 1, 2, \dots$  of eigenvalues  $\beta_{n,p}$ . We can now apply the initial conditions to obtain the amplitude of each solution. For the  $z$ -axis we get

$$A_m^+ = \frac{2}{L} \frac{1}{1 + \text{sinc}(\eta_m^+ L)} \cos \left[ \eta_m^+ \left( z_0 - d - \frac{L}{2} \right) \right] \quad (16)$$

$$A_m^- = \frac{2}{L} \frac{1}{1 - \text{sinc}(\eta_m^- L)} \sin \left[ \eta_m^- \left( z_0 - d - \frac{L}{2} \right) \right], \quad (17)$$

while for the radial and angular parts we obtain

$$A_{n,p} = \frac{(\beta_{n,p} R)^2 J_n(\beta_{n,p} \rho_0) \exp(in\phi_0)}{\pi R^2 \left[ \left( \frac{dR}{D\tau_{\text{ev}}} \right)^2 + (\beta_{n,p} R)^2 - n^2 \right] J_n(\beta_{n,p} R)}. \quad (18)$$

Then, the full propagator is

$$P(\rho, \phi, z, t) = \frac{L}{V} \sum_{m=1}^{\infty} \sum_{n=-\infty}^{\infty} \sum_{p=0}^{\infty} \left\{ A_m^- \sin \left[ \eta_m^- \left( z - d - \frac{L}{2} \right) \right] + A_m^+ \cos \left[ \eta_m^+ \left( z - d - \frac{L}{2} \right) \right] \right\} \times \beta_{n,p} \rho J_n(\beta\rho) \exp[-in(\phi - \phi_0) - D(\beta_{n,p}^2 + \eta_m^2)t], \quad (19)$$

from which we can obtain the autocorrelation by numerically calculating the different eigenvalues from the transcendental equations and integrating the propagator within the confinement volume, following Eq (2). Note that the integral over the angular coordinates  $\phi$  and  $\phi_0$ , together with the spherical harmonics normalization condition, yields  $4\pi^2 \delta_{n,k}$ , with  $k$  the specific dipole-dipole interaction term on resonance considered, which for us, being the flip-flop (or ZZ) term, yields  $k = 0$ , which replaces the sum over  $n$ . Then

$$G^{\text{ev}}(t) = \frac{8\pi^2 \Upsilon^2}{V} \sum_{m=1}^{\infty} \sum_{p=0}^{\infty} \frac{(\beta_p R)^2}{[(\eta_0 R)^2 + (\beta_p R)^2] J_0^2(\beta_p R)} \exp\left(-\frac{t}{\tau_{m,p}}\right) \times \left( \int_0^R d\rho \cdot \rho \int_d^{d+L} dz Y_2^{(k)}(z, \rho) J_k(\beta_{k,p} \rho) \left\{ \frac{\sin[\eta_m^-(z_0 - d - \frac{L}{2})]}{1 - \text{sinc}(\eta_m^- L)} \sin\left[\eta_m^-\left(z - d - \frac{L}{2}\right)\right] + \frac{\cos[\eta_m^+(z_0 - d - \frac{L}{2})]}{1 + \text{sinc}(\eta_m^+ L)} \cos\left[\eta_m^+\left(z - d - \frac{L}{2}\right)\right] \right\} \right)^2, \quad (20)$$

where we denote  $\beta_p \equiv \beta_{n=0,p}$  for simplicity. Note as well that the coefficients  $\tau_{m,p} = 1/D(\beta_p^2 + \eta_m^2)$  in Eq. (20) describe the different decay modes of the correlation function.

#### IV. RESULTS

We now explicitly calculate the correlation function in the sticky walls and evaporating walls scenarios, for different confining cylinder volumes, and various evaporation rates. We benchmark the results with the ideal case of perfectly reflective walls and advance the implications for experiments of each of the models.



### A. Sticky walls

In the ideal scenario in which molecules rebound from the walls of the confining volume, with the nuclei retaining the spin orientation after the collision, the correlation signal detected by the NV-center follows the diffusion process up to the volume time  $\tau_V$ , that marks the onset of a *plateau* in which the correlation remains constant in time and diffusion has no further effect on the statistical polarization of nuclei. In this limit, the correlation function can be calculated exactly by integrating a uniform distribution of nuclei in the region. Following Ref. [25] the exact equation is

$$G^{\text{ideal}}(t \gg \tau_V) = \frac{4\pi^2\Upsilon^2}{V} \left[ \int_0^R \int_d^{d+L} d\rho dz \frac{\rho Y_2^0(\rho, z)}{(\rho^2 + z^2)^{3/2}} \right]^2, \quad (21)$$

whose functional form gets simplified if we consider the angular relation between the lower and upper borders of the cylinder confining region. Taking the NV center position as the lower vertex of two triangles of sides  $R$ , and  $d$  or  $d+L$  along the cylinder axis, and whose long side is the distance between the NV center and the borders of the cylinder lower or upper cap, we can define  $\alpha$  and  $\beta$  to be the angles between said long sides and the alignment axis, as shown in Fig. 1, and whose cosines are  $\cos \alpha = R/\sqrt{d^2 + R^2}$  and  $\cos \beta = (d+L)/\sqrt{(d+L)^2 + R^2}$ . Then, the amplitude of the *plateau* is [25]

$$G^{\text{ideal}}(t \gg \tau_V) = \frac{4\pi^2}{V} (\cos \beta - \sin \alpha)^2. \quad (22)$$

When the confining volume walls are sticky, the nuclei that end trapped on the walls will continue contributing to the overall correlation signal from that fixed position. As diffusion proceeds, eventually, all nuclei will be attached to the confining volume walls. Then, the correlation signal will also reach a *plateau*, with an amplitude that depends on the specific surface to volume ratio of the confinement region. Solving analytically Eq. (5) and using the same angles definitions as previously, we get that

$$G^{\text{sticky}}(t \gg \tau_V) = \frac{2\pi^2}{SR} (\cos \beta - \sin \alpha) [2 \cos^3 \alpha + 2 \sin^3 \beta + \sin(2\alpha) - \sin(2\beta)]. \quad (23)$$

The *plateau* section of the correlation function is crucial for parameter estimation, as any signal whose decay is described by said correlation behaves, upon reaching the flat section, as a coherent signal. It is, therefore, ideal for spectroscopy. As well, the full behavior of the correlation function is interesting in itself, as it contains information about the different physical processes undergone by the confined sample. The full correlation evolution in the sticky model requires numerically integrating Eq. (8). In Fig 2 we display the correlation function corresponding to four different confining volumes with sticky walls, together with the asymptotic behavior Eq. (22) for the ideal *plateau* section of the correlation, and the different physical regimes that the sample goes through.

The early time behavior of the correlation function is dominated by free diffusion, as evidenced by the comparison with the correlation function of a freely diffusing fluid, which is governed by the equation [31]

$$G^{\text{free}}(\tilde{t}) = \frac{4\Upsilon^2}{\sqrt{\pi}} \left[ \left( -\tilde{t}^{-3/2} + \frac{3\tilde{t}^{3/2}}{2} + \frac{1}{\sqrt{\tilde{t}}} - \frac{7\sqrt{\tilde{t}}}{4} \right) \sqrt{\frac{\pi}{\tilde{t}}} \operatorname{erfc} \left( \frac{1}{\sqrt{\tilde{t}}} \right) \exp \left( \frac{1}{\tilde{t}} \right) + \tilde{t}^{-3/2} - \frac{3}{2\sqrt{\tilde{t}}} - \frac{3\sqrt{\pi}\tilde{t}}{2} + 3\sqrt{\tilde{t}} + \frac{\sqrt{\pi}}{4} \right], \quad (24)$$

with scaled time parameter  $\tilde{t} = t/T_D$ . Eq. (24) features two distinct regimes. The first, corresponding to the short times  $t \ll T_D$ , presents a fast decay  $\sim \exp(-6t/T_D)$ , while in the second, at long times  $t \gg T_D$ , the scaling is  $\sim (t/T_D)^{-3/2}$ . We can see from Fig. 2 that Eq. (8) exactly reproduces this trend at early times, deviating only when the molecules start arriving at the walls and the regime changes from free to confined diffusion. Moreover, we observe that it is only for the largest confinement volumes that the asymptotic power-law behavior is fully realized. This both confirms the validity of our calculation of the sticky regime, and provides valuable information about the behavior of the confined sample and, crucially, about the confinement region itself.

The long-time behavior shows the characteristic *plateau* from confinement, whose amplitude is, in Fig. 2, comparably smaller than in the ideal reflective walls scenario. Both the onset time of this *plateau*, defined as  $\tau_V$ , and its amplitude, are crucial for confined nano-NMR applications. To quantify the difference between ideal and sticky confinement, we can define the ratio between the long time behavior of both as

$$\frac{G^{\text{sticky}}(t \gg \tau_V)}{G^{\text{ideal}}(t \gg \tau_V)} = \frac{L}{4(L+R)} \frac{2 \cos^3 \alpha + 2 \sin^3 \beta + \sin(2\alpha) - \sin(2\beta)}{\cos \beta - \sin \alpha}, \quad (25)$$

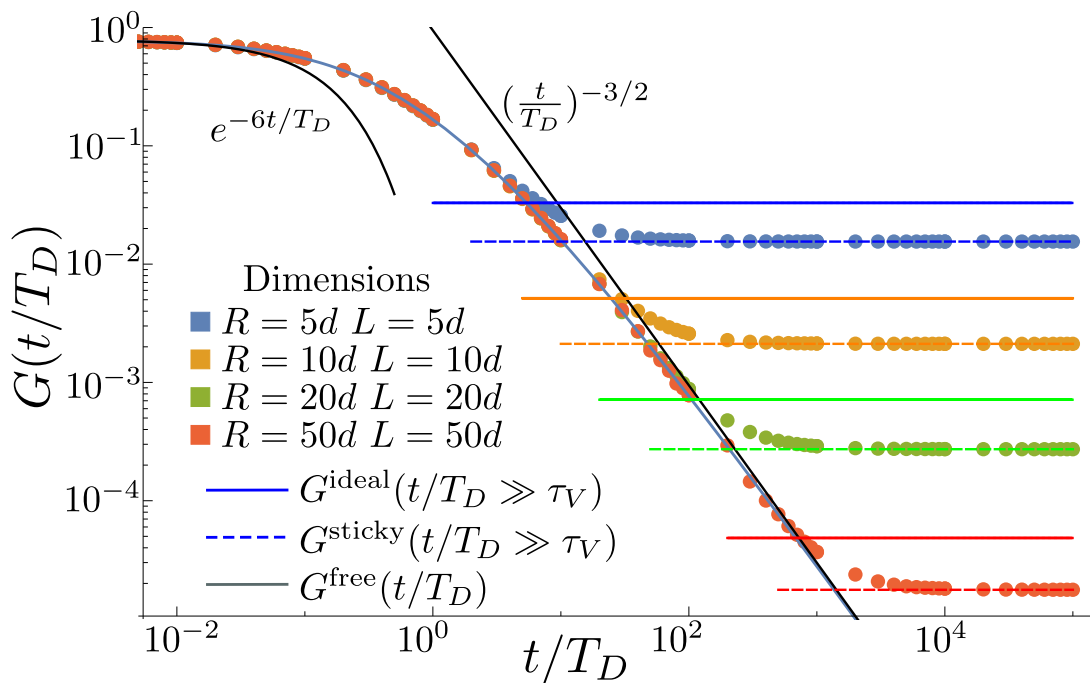


Figure 2. Logarithmic scale time evolution of the correlation function Eq. (8) for confined nano-NMR with sticky walls (dots), for different confinement volumes. Asymptotic behavior of the correlation function in the confinement regime for both the ideal, completely reflective walls [Eq. (22), full horizontal lines] and fully sticky walls [Eq. (23), dashed horizontal lines], calculated exactly. Early time diffusive behavior and asymptotic time-dependence of the diffusive regime of the sample are displayed as solid, black lines labeled with the corresponding time-dependence, and the free diffusion behavior, described by Eq. (24) shown as a solid Grey line. Note that we use units normalized to the NV center depth  $d$  and diffusion time  $T_D = d^2/D$ , to display the universal behavior.

which we can use to estimate whether having sticky walls could prove to be, at any point, advantageous. Fig. 3 shows this ratio between amplitudes for significant confinement volumes.

The amplitude of the signal in either confinement regime discussed depends on the cylinder size and the depth of the NV center probe. If the radius  $R \gg L$  the height of the cylinder, then, the prefactor in Eq. (25) goes to zero. As well, in this limit, from the definition of the angles  $\alpha$  and  $\beta$ , we can take  $\beta \approx 90 - \alpha$ , which means that the amplitudes ratio reduces to  $\approx \cos^3 \alpha / (1 + R/L)$ . Since the cosine cannot be greater than 1, for flatter cylinders, ideally reflective walls will always yield a signal whose *plateau* amplitude will be greater than having sticky walls.

On the opposite scenario, when  $L \gg R$ , the prefactor in Eq. (25)  $\sim 1/4$ , while in the angular part, the angle  $\beta \rightarrow 0$ , yielding a ratio  $\approx [\cos^3 \alpha - \sin(2\alpha)] / (2 - 2 \sin \alpha)$ , which then depends on the specific radius and the depth of the probe, as they define the angle  $\alpha$ . For very shallow NV centers, in which the radius is several times the depth,  $\alpha$  is small and the ratio approximates  $1/2$ , favoring reflective walls. On the other hand, if the cylinder is narrow compared with the depth of the probe, then the ratio has hyperbolic growth, meaning that narrow cylinders with deep probes favor sticky walls over reflective, ideal walls, as shown in Fig. 3.

For spectroscopy, the best scenario is always to have as large a signal amplitude as possible, and to reach the *plateau* as early in the dynamics as can be managed, to benefit from the absence of diffusion induced decay of the signal in this region. Eq. (25) can be used to determine, given a constructed confinement region, whether the optimal strategy is to make the walls sticky, or rather as reflective as possible. Moreover, Eqs. (22) and (23) can be used to determine the ideal cylinder confining volume parameters for a given NV center depth, such that the amplitude of the *plateau* is maximized. For reflective walls, these parameters are  $R \approx 0.93d$  and  $L \approx 0.88d$ , while in the case of sticky walls, the ideal parameters are  $R \approx 0.82d$  and  $L \approx 0.92d$ . We observe that the optimal design in terms of *plateau* amplitude is, to a good approximation, having a symmetric cylinder. The same optimal values determine the earliest time in which the *plateau* region is reached.

A prime forecasted application of nano-NMR is the ability to capture the dynamics of diffusion processes at the nanoscale [31], from which the diffusion coefficient of fluids can be accurately estimated [40]. Typically, the diffusion coefficient is determined by fitting the decay shape of the experimental correlation to an exponential function  $\sim \exp(-t/T_D)$ , with  $T_D$  defined as the life-time of the exponential. Taking  $T_D = d^2/D$ , yields the diffusion coefficient  $D$ . Yet the exponential model is just an approximation for diffusion at the nanoscale, valid, as we readily observe from



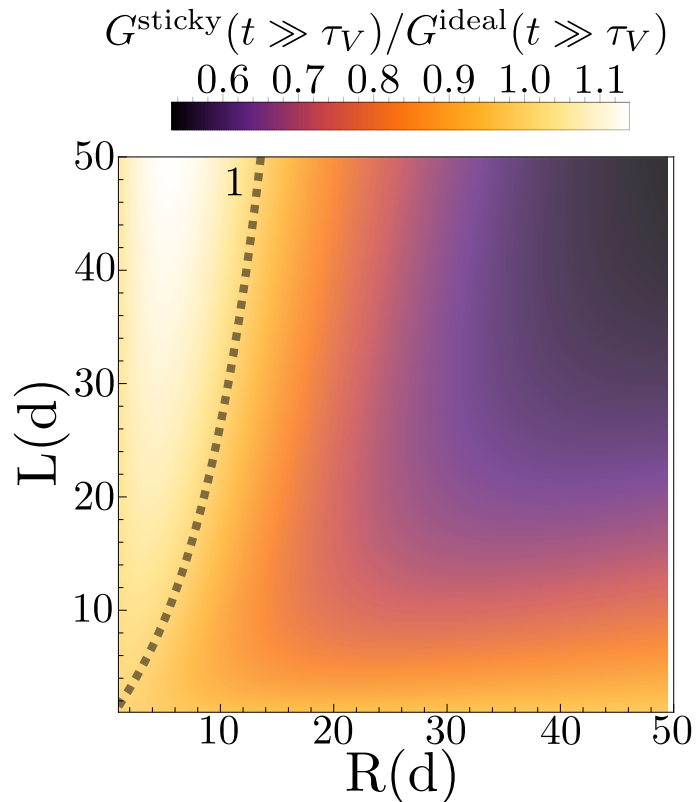


Figure 3. *Plateau* amplitude ratio between correlations in the sticky and completely reflective cases, as defined by Eq. (25). Here, we choose a depth  $d = 15$  nm, typical of nano-NMR experiments with NV centers [40], and display the ratio as a function of the confinement cylinder size, defined by its radius  $R$  and height  $L$ . We observe a marked distinction for asymmetric cylinders, such that when the depth is much greater than the width, sticky walls provide a greater amplitude. On the other hand, wider cylinders favor as reflective walls as possible. As the confinement volume grows, the ratio goes asymptotically to  $1/2$ . The thick, dashed line marks the boundary of equal *plateau* amplitude.

Fig. 2, only at early times, and then the exponent is, rather,  $\sim \exp(-6t/T_D)$  for three-dimensional diffusion. The long-time behavior of free diffusive fluids following a power-law, which from Eq. (24) is  $G^{\text{free}}(t \rightarrow \infty) = 32t^{-3/2}/15\sqrt{\pi}T_D^{-3/2}$ . Then, since the fitting occurs to an imprecise model, inaccuracies in estimating  $D$  occur.

On the other hand, sample confinement results in correlations which, after some characteristic time  $\tau_V$ , no longer decay, meaning that, on average, no diffusion is happening in the sample. The transition from an early time diffusive regime and a long time confined regime is smooth, as shown in Fig. 2, but given the analytical expressions derived for the *plateau* amplitude in Eqs. (22) and (23), and the asymptotic behavior of the free diffusion model at long times, we can easily calculate the volume time  $\tau_V$  that marks the transition between regimes at the crossing time between the two regimes, yielding

$$\tau_V = \left[ \frac{32}{15\sqrt{\pi}G^{\text{ideal,sticky}}(t \gg \tau_V)} \right]^{2/3} T_D. \quad (26)$$

This time can be accurately estimated in experiments from the crossing point of the decaying and flat sections of the correlations. Knowing the depth of the probe, which can be estimated from power spectrum measurements [41], and using the definition of the diffusion time as  $T_D = d^2/D$  we get that

$$D = \left[ \frac{32}{15\sqrt{\pi}G^{\text{ideal,sticky}}(t \gg \tau_V)} \right]^{2/3} \frac{d^2}{\tau_V}, \quad (27)$$

yielding a precise measurement of the diffusion coefficient  $D$  of the fluid. Moreover, the successful experiment targeting the diffusion coefficient requires, contrary to the case for spectroscopy, a large confinement volume that allows for a larger diffusive regime in which the power-law behavior is more exactly achieved.

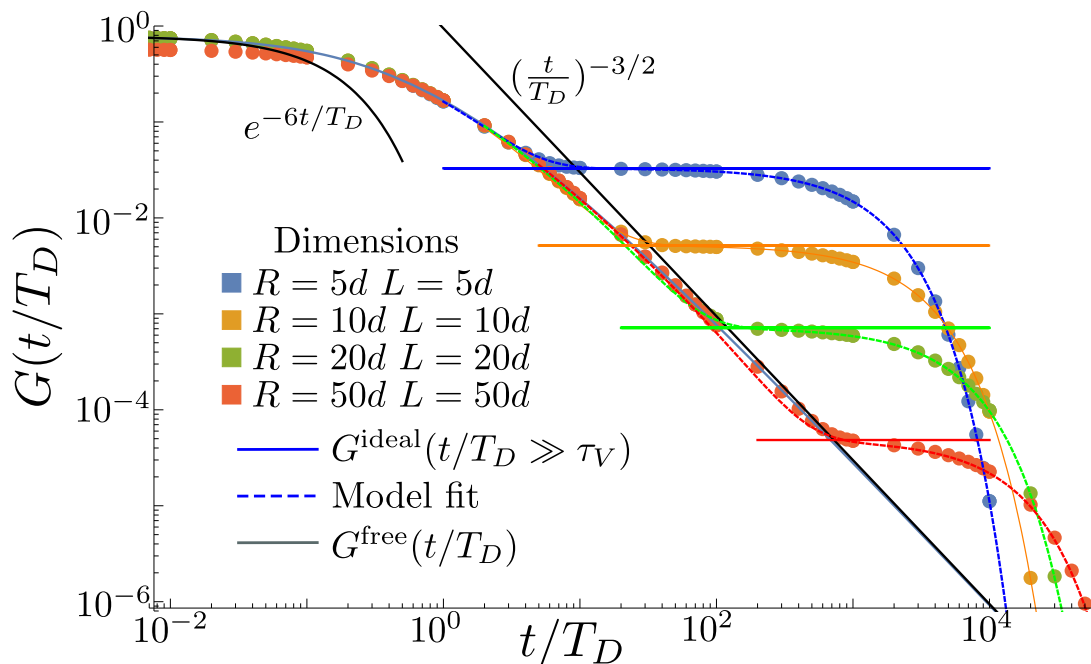


Figure 4. Logarithmic scale time evolution of the correlation function for a confinement volume with evaporating walls, calculated from Eq. (20), considering  $\tau_{\text{ev}} = 1000T_D$  and various confinement volumes (dots). For reference, the free diffusion correlation function Eq. (24) is shown as a grey line on the background, and its asymptotic behavior at very short and very long times as black lines labeled with the corresponding time dependence. As well, the ideal reflective walls *plateau* amplitude from Eq. (22) is shown as a horizontal solid line for each of the volumes considered. The model fitted to each of the correlation functions is shown as dashed lines, and corresponds to Eq. (28), with the appropriate rates adjusted according to the different confinement volumes considered. Note that we use units normalized to the NV center depth  $d$  and diffusion time  $T_D = d^2/D$ , to display the universal behavior.

## B. Dissipating walls

We now consider the scenario in which the walls cause a decay of the correlations due to, for example, seepage of the nuclei out of the confinement volume [26], or as a result of orientation changes in the nuclei upon interaction with the walls. The correlation function in this scenario is calculated by numerically solving Eq. (20), which comprises of solving two transcendental equations and calculating (truncated) infinite sums. To do so, we first numerically solve Eq. 15, and truncate the list of solutions by calculating the decay coefficients to which each of them leads, taking only the fastest 100 decaying modes. The procedure is analogous with the transcendental equation 14 solutions that result in the eigenvalues  $\eta_m$ . We then calculate all the relevant terms in the sum and, with them, the correlation function for different confinement volumes and dissipation rates.

In Fig. 4, we display the correlation function corresponding to a fixed dissipation rate  $\tau_{\text{ev}} = 1000T_D$  and four different confinement volumes, together with the correlation function envelope Eq. (24) that describes the free diffusion scenario, and its asymptotic behavior at very short and long times. For all confinement volumes considered, we observe three distinct regions. The first one is described by free diffusion, and behaves exponentially at the very beginning, showing the characteristic power-law behavior of free diffusion at later times, which is more pronounced whenever the confinement volume is bigger, as the influence of the walls is slower to appear.

As the nuclei reach the walls of the confinement volume, they either rebound and continue contributing to the correlation, or dissipate at a given rate which, in Fig. 4, is  $\tau_{\text{ev}} = 1000T_D$ , and that is responsible for further decay of the correlations. Said decay is well captured by a simple model that combines early time free diffusion with a long time characteristic confinement *plateau* that decays exponentially at a rate that is, to a very good approximation, the slowest decaying mode in Eq. (19), which dominates by orders of magnitude over all the other modes present, and which approximates  $\tau_{0,0} \approx Sd/V\tau_{\text{ev}}$ , as we demonstrate analytically in Appendix C. There, we also show the dominance of the  $\tau_{0,0}$  mode and the regime of validity. To describe the transition between diffusive and dissipative-confinement regimes, the free diffusion correlation from Eq. (24) includes as well an exponential term that accounts for the decay of diffusion as more nuclei rebound on the walls and re-enter the sensing region, leading to the *plateau*. Diffusion decay can be understood through a half-life for the nuclei to reach the walls, which relates to the volume

time that marks the crossover between diffusion and confinement regimes as  $2/\tau_V$ . Then

$$G^{\text{ev}}(t) \approx B_{\text{rms}}^2 G^{\text{free}}(t/T_D) \exp(-\frac{2t}{\tau_V}) + G^{\text{ideal}}(t \gg \tau_V) \exp\left(-\frac{Sd}{V\tau_{\text{ev}}}t\right). \quad (28)$$

Note that the  $B_{\text{rms}}^2$  is the initial amplitude of the signal [see Eq. (A18) in Appendix A]. Thus, a simple model composed of two parameters accurately describes the complex dynamics of the evaporating confined fluid.

Evaporation causes a rapid degrading of correlations. Eq. (28) tells us that, whenever the dissipation time is sufficiently long compared to the diffusion time, the *plateau* region characteristic of confinement will be reached before dissipation has a significant effect on the signal. On the contrary, for larger volumes, said *plateau* is hardly achieved but, on the other hand, dissipation happens at a slower rate, as nuclei take longer to reach the walls. The factor  $Sd/V$ , that modulates  $\tau_{\text{ev}}$  in Eq. (28), leads to an optimal trade-off between dissipation on the surface and diffusion on the bulk, where the design of the confinement volume can be tailored to the given dissipation rate that the walls are known to induce, to minimize its impact through maximizing the volume for a given surface, or minimizing the surface for a given volume. Moreover, it is potentially useful again to estimate the diffusion coefficient of the fluid sample. As Eq. (28) describes well the transition point between pure diffusion and the effect of the walls at  $\tau_V$ , much like in the case of sticky walls. Here we find again a situation where a bigger confinement yields a better estimation of  $D$ . It also tells us that in the case of combined effects, sticky and dissipative regimes, we can find a simple expression to describe the long time evolution of the correlation, by replacing  $G^{\text{ideal}}$  by  $G^{\text{sticky}}$  in Eq. (28).

Spectroscopy demands stability of the correlation function, with the rate of decay of correlations typically controlling the minimum estimation error attainable [42]. In Fig. 5, we fix the parameters of the confinement volume to  $R = L = 5d$ , and study the influence of different dissipation rates, varying in powers of ten, from  $\tau_{\text{ev}} = T_D$  to  $\tau_{\text{ev}} = 10^6 T_D$ , to observe the onset of the *plateau* region in which the signal behaves coherently, and its disappearance due to dissipation. For slow dissipation rates  $\tau_{\text{ev}} \gg T_D$ , the transition from diffusion to confinement and dissipation is well described by our model in Eq. (28) but, for dissipation rates which are on the order of the characteristic diffusion time, things are more complicated, as shown by the results for  $\tau_{\text{ev}} = T_D$  and  $\tau_{\text{ev}} = 10T_D$ , for which the simple model for the long time behavior of correlations represented by Eq. (28) overestimates the decay of correlations. The reason is that, when diffusion and dissipation have similar rates, their behavior cannot be as easily disentangled, as it is evident by the fact that the definition of  $\tau_V$  is not valid anymore, and which also shows in the fact that no decay eigenvalue  $\tau_{n,m}$  dominates significantly. Fast evaporation prevents the usefulness of confinement for the purpose of nano-NMR spectroscopy.

To explore the regime in which diffusion and dissipation are commensurate, we calculate, in Fig. 6, the behavior of the correlation for fast dissipation rates, ranging from  $\tau_{\text{ev}} = T_D$  to  $\tau_{\text{ev}} = 20T_D$ . We observe that, compared to the correlation function corresponding to free diffusion Eq. (24), which accurately describes the initial time behavior when dissipation rates are slow, as shown in Fig. 5, here, the decay of correlations that is induced by free diffusion underestimates the overall decay, even at early times. The intuitive reason is that, in this scenario, as soon as nuclei reach the walls of the confinement volume, they evaporate, and stop contributing to the overall magnetic field. The mathematical reason is that we no longer have a mode  $\tau_{m,p}$  that dominates. Rather, many decay modes contribute on the same order of magnitude. Moreover, we no longer have a clear definition of  $\tau_V$  that separates the diffusive and confinement regimes. Overall, the meaning is that in this scenario diffusion and evaporation mingle and act concurrently. In this case, a bigger confinement volume, such as those shown in Fig. 4, in which the effect of the walls is delayed due to the nuclei taking longer to reach them, could help disentangling the mixture of evaporation and diffusion.

## V. IMPLICATIONS FOR FREQUENCY RESOLUTION

The actual physics governing confined diffusion at the nanoscale, as displayed by the correlation function, is likely to be a combination of the noise models described in this article, with the confining volume walls inducing a decay of the correlation function on some time-scale  $\tau_{\text{ev}}$ , as captured by the evaporating model, while at the same time slowing diffusion due to interaction with the nuclei in the sample, as described by the sticky model. The particular details of the exact model can be elucidated from experiments by comparing with the calculations shown above. In this section, we focus on a rather different implication of the realistic behavior of the correlation function of a confined sample. Namely, its usefulness for spectroscopy. In particular, we concentrate the ensuing discussion on frequency estimation.

The ability to estimate a parameter from a signal depends on various things: the particular experiment, sensor, and protocol used to detect the signal, the underlying noise model, and the choice of data analysis. For nano-NMR spectroscopy with NV centers, in which the statistical polarization is subjected to diffusion noise, the best known protocols are those of the phase-sensitive family [13, 43], such as Qdyne [44], which maximize frequency information extraction as benchmarked by the Fisher information [45].

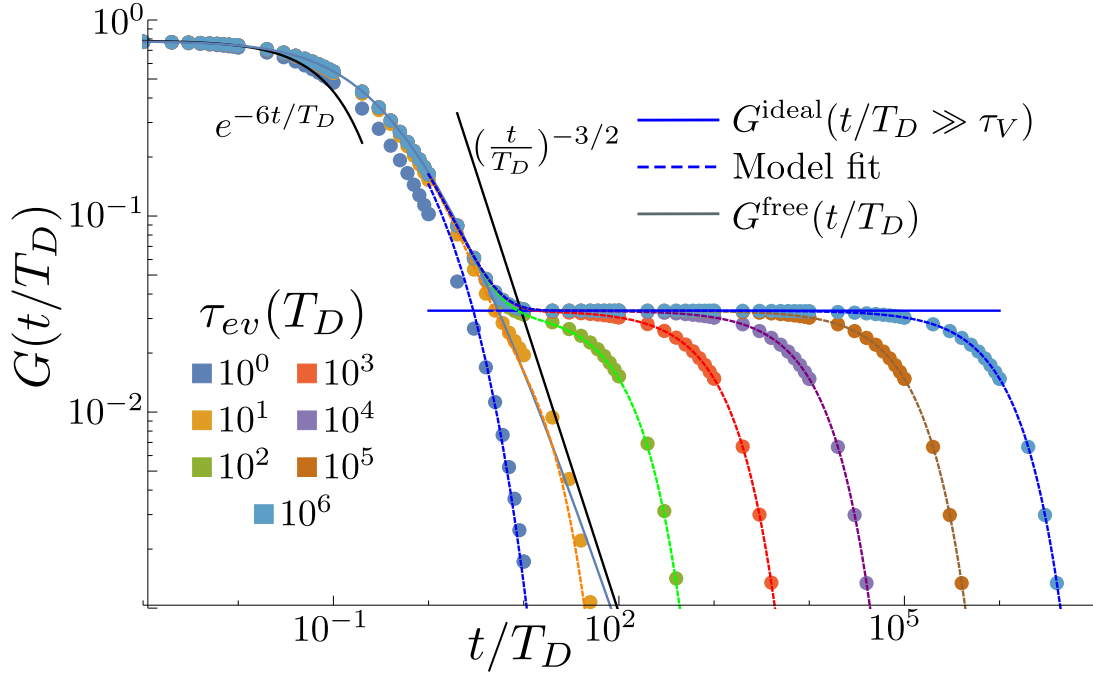


Figure 5. Logarithmic scale time evolution of the correlation function for a confinement volume with evaporating walls, calculated from Eq. (20) by considering a fixed confinement volume of size  $R = 5d$  and  $L = 5d$ , and varying the evaporation rate  $\tau_{ev}$  in powers of ten (dots). Free diffusion correlation function Eq. (24) (solid Grey line) and its asymptotic behavior at very short and very long times (solid black lines). Ideal reflective walls *plateau* from Eq. (22) for the volume considered, showing that the *plateau* is achieved for slow evaporation. The model fitted to each of the correlation functions corresponds with Eq. (28), with the appropriate rates adjusted according to the different confinement volumes considered. Note that for this confinement volume  $S/V = 1/5d$  and that  $\tau_V \approx 11T_D$ , and that we use units normalized to the NV center depth  $d$  and diffusion time  $T_D = d^2/D$ , to display the universal behavior.

According to the Crámer-Rao bound, the Fisher information for a given parameter lower bounds the minimum error attainable in estimating said parameter from a given experiment. The Fisher information on a parameter  $\delta$  given a discrete distribution  $\{P_i(\delta)\}_i$  is calculated as

$$I_\delta = \sum_i \frac{\left(\frac{dP_i}{d\delta}\right)^2}{P_i}, \quad (29)$$

where in our case  $\delta$  represents the (typically small) frequency to be estimated, and  $P_i$  is the probability of the quantum sensor to be found at the state  $i$ , measured as the average fluorescence. For a signal coming from statistically polarized diffusing nuclei, these probabilities directly relate to the auto-correlation of the magnetic field, such that

$$P = \frac{1 + \Phi_{\text{rms}}^2 \cos(\delta t) G(t/T_D)}{2} \quad (30)$$

is the probability of finding the prove in its original state, with  $\Phi_{\text{rms}} \propto B_{\text{rms}}$ . For free diffusion, in which the correlation function envelope  $G^{\text{free}}(t/T_D)$  in Eq. (24) follows a power-law at long times [31, 40], the Fisher information scaling with the total duration  $T$  of an experiment is  $I_\delta^{\text{free}} \propto T \log(\delta T)$  [42]. Then, a sufficiently long total measurement time  $T$  permits estimating small frequencies. On the other hand, an ideal confinement, with perfectly reflective walls or perfectly sticky walls, in which the correlation envelope reaches the *plateau*, recovers the coherent signal limit, in which the oscillations do not decay [25]. Then, the Fisher information is  $I_\delta \propto T^3$  [46], albeit with a decreased amplitude which corresponds the *plateau* amplitude, which can be significantly smaller than the  $B_{\text{rms}}$ . Consequently, either ideally reflective or sticky walls, combined with moderately sized confinement volumes where the *plateau* amplitude is just one or two orders of magnitude smaller than the  $B_{\text{rms}}$  (see Fig. 2), mean that using moderate total measurement times  $T$ , a confinement spectroscopy experiment is a better strategy in terms of frequency estimation, particularly at low frequencies  $\delta < \pi/T_D$ . The Fisher information ratio between a sticky walls confinement and a free diffusion

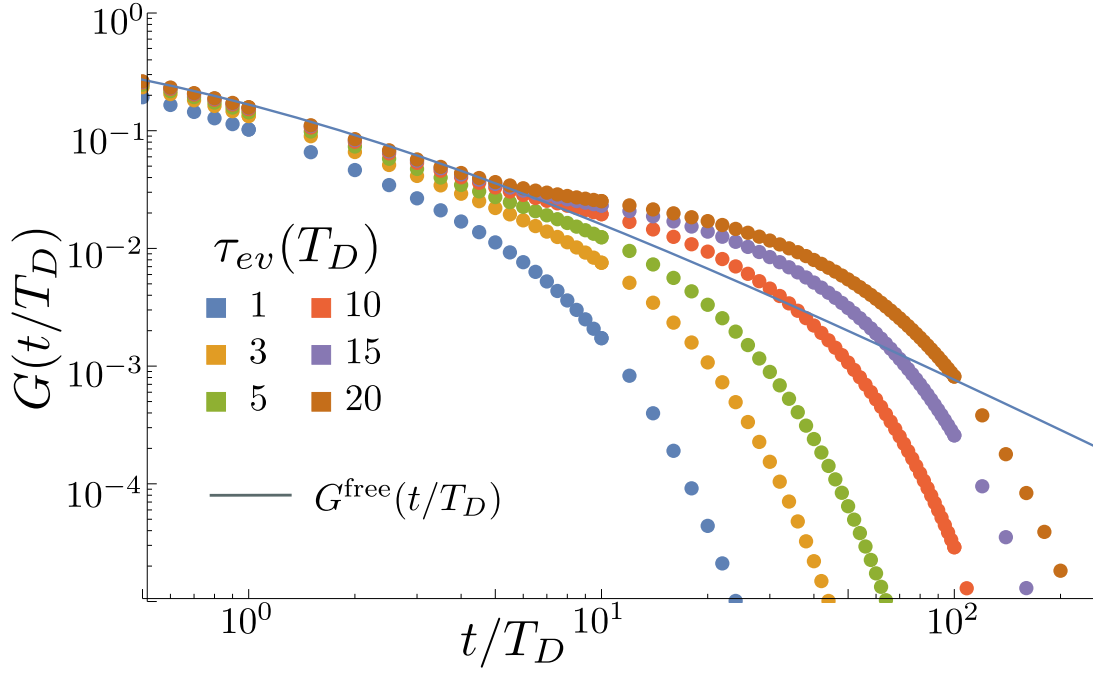


Figure 6. Logarithmic scale time evolution of the correlation function for confinement with fast evaporating walls, calculated from Eq. (20). In this figure, the confinement cylinder volume features  $R = 5d$  and  $L = 5d$ , and the evaporation rate ranges from  $\tau_{ev} = T_D$  to  $\tau_{ev} = 20T_D$ . In gray, free diffusion correlation function Eq. (24). Here, we can no longer find a simple model that reproduces the behavior of the correlations with time, nor we can see a distinction between diffusive and evaporating regimes. Note that we use units normalized to the NV center depth  $d$  and diffusion time  $T_D = d^2/D$ , to display the universal behavior.

experiment is

$$\frac{I_\delta^{\text{sticky}}}{I_\delta^{\text{free}}} \approx \frac{[G^{\text{sticky}}(t \gg \tau_V)]^4 T^2}{\Phi_{\text{rms}}^4 T_D^2 \log \delta T}, \quad (31)$$

where we assume the long experiment time limit  $T \gg \tau_V$ , and where for fully reflective walls  $G^{\text{ideal}}(t \gg \tau_V)$  replaces  $G^{\text{sticky}}(t \gg \tau_V)$ .

Eq. (31) shows that free diffusion nano-NMR yields better frequency resolution only for very viscous fluids or exceedingly large confinement volumes. However, Eq. (31) disregards the possibility that the walls induce a decay of the correlations. Therefore, a more realistic comparison would be to consider a correlation function for the confinement regime which accounts for both sticky and evaporating walls, for which we can use the approximate expression Eq. (28). In this case, the exact expression for the Fisher information is quite involved (see Eq. (D7) in Appendix D), but can be studied in certain limits. In particular, we are interested in the limits of very fast and very slow evaporation.

When the walls induce a very fast decay of the correlations because  $\tau_{ev} \leq T_D$ , the sample behaves, essentially, as a free diffusing fluid which suffers from an additional noise term rather than diffusion on the time-scale of the evaporation time  $\tau_{ev}$ , and which causes added exponential correlation decay. Then, the Fisher information ratio between a confined and a free sample spectroscopy experiment is

$$\frac{I_\delta^{\text{ev}}}{I_\delta^{\text{free}}} \approx \frac{\log(1 + \tau_{ev}^2 \delta^2 + \tau_{ev}^4 \delta^4)}{8 \log \delta T}, \quad (32)$$

which explicitly demonstrates that, in this scenario, the best strategy is to not use confinement.

For large evaporation times  $\tau_{ev} \gg \{T_D, T_V\}$ , it is instructive to explicitly show the approximate Fisher information expression for confined nano-NMR spectroscopy. To calculate it, we use the approximate model Eq. (28), which yields:

$$I_\delta^{\text{ev}} \approx \frac{[G^{\text{ideal}}(t \gg \tau_V)]^4 \tilde{\tau}_{ev}^2}{16\tilde{\tau}^2} \left[ 2\tilde{\tau}_{ev}T + 2T^2 \exp\left(-\frac{2T}{\tilde{\tau}_{ev}}\right) \right] \tanh(\delta^2 \tilde{\tau}_{ev}^2), \quad (33)$$

with  $\tilde{\tau}_{ev} = V\tau_{ev}/Sd$ .

Eq. (33) features two distinct, important regimes, that depend on the specific target frequency  $\delta$  and total measurement time  $T$ . In particular, Eq. (33) shows that the information about the frequency grows quadratically during the *plateau* phase of the time evolution of the correlation function, becoming linear when  $T > \tau_{\text{ev}}$ . As the hyperbolic tangent behaves as  $\tanh x \sim x$  when  $x \rightarrow 0$ , this means that a resolution limit for small frequencies exists when  $\delta < \pi/\tau_{\text{ev}}$ . On the other hand,  $\tau_{\text{ev}}$  can be substantially large, which not only provides with a large measurement time  $T$  of quadratic information accumulation but, importantly, it also means that even for quite small frequencies, sample confinement is a better strategy than having free diffusion, as the Fisher information comparison shows:

$$\frac{I_{\delta}^{\text{ev}}}{I_{\delta}^{\text{free}}} \approx \frac{[G^{\text{ideal}}(t \gg \tau_V)]^4 \tau_{\text{ev}}^2 T}{16\Phi_{\text{rms}}^4 T_D^3 \log \delta T}. \quad (34)$$

Since  $\tau_{\text{ev}} \gg T_D$  for good confinement, for frequencies  $\delta \geq \pi/\tau_{\text{ev}}$ , confining the sample minimizes the frequency estimation error. For extremely small frequencies, Eq. (33) goes to zero, which means that the logarithmic behavior  $\log(\delta T)$  of the Fisher information for free diffusion confers this strategy, in principle, with an advantage, despite requiring extremely long measurement times  $T$  to reduce the estimation error. This can be inferred from Fig. 5, where the gentler slope of the free diffusion correlation means that it eventually crosses with the faster decay of evaporation, albeit at a very long time and exceedingly small amplitude.

Summarizing, sample confinement provides an advantage for NMR spectroscopy of nano-sized samples for fair sized confinement volumes on the order of  $10^3 \text{nm}^3$ , and whose dephasing time due to interaction of the nuclei with the walls or due to seepage is large  $\geq 1 \text{s}$ . For very large confinement volumes  $\sim 0.1 \mu\text{m}^3$  or fast dephasing times  $\leq 100 \mu\text{s}$ , an unconfined experiment has a larger chance of success. For medium confinement volumes or dephasing times, which experiment yields the smallest estimation error can be predicted quite accurately using the formulas calculated here.

## VI. CONCLUSIONS

Realizing sample confinement is a promising route to perform NMR spectroscopy on fluid samples with quantum sensors. A first experimental demonstration of actual confinement would require showing the characteristic *plateau* that occurs when the diffusive regime transitions to the confined regime. In this article, we have modeled different confinement effects that can substantially modify the ideal behavior of the correlations. By calculating the effect of having sticky walls, which slow diffusion close to the borders of the confinement region, we show how the amplitude of the *plateau* can significantly change, not necessarily decreasing, and by calculating the effect of walls that induce dephasing or are porous, we demonstrate that the *plateau* decays with time. A simplified model that combines both effects, when the evaporation time is sufficiently different from the diffusion time, can be described by a simple expression that we provide, and which can be used to predict the behavior of the correlations for a given experiment, or to elucidate the properties of the experiment based on the observed correlations. Additionally, we provide exact expressions for estimating the diffusion coefficient, and to calculate the frequency estimation error for precision spectroscopy.

Recently, a first attempt at experimental sample confinement was published by Liu et al. [26], where using a metal-organic framework they managed to slow diffusion to a trickle, greatly improving the frequency estimation ability by substantially reducing the width of the power spectrum of the sample. This seminal work demonstrates that metal-organic frameworks could be a nice strategy for sample confinement, as they can, essentially, be designed to have the desired mesh holes size, which means any confinement volume could be engineered. Our evaporation model describes accurately the effect of such a framework, where diffusion of molecules out of the confinement volume still happens, but at a much slower rate than that of free diffusion. Furthermore, this result has been followed, lately, by various successful attempts at partial confinement in assorted setups which demonstrate great improvement in slowing water diffusion, and uncover interesting behaviors regarding surface interactions or evaporation [47–49], hinting at the importance of having reliable, accurate models capable of describing the unexpected behavior that confined liquids at the nanoscale can show.

The models presented here open up the pathway to understand realistic sample confinement, and generate the foundation to study more complicated diffusion effects through a mixture of analytical and numerical techniques. The interface between the diffusive and confinement regimes permits determining the diffusion coefficient of a fluid with improved accuracy, and an appropriate confinement can lead to enhanced resolution in nano-NMR spectroscopy.

## VII. ACKNOWLEDGEMENTS

We are grateful to Alex Retzker for fruitful discussions. S.O.-C acknowledges the support from the *María Zambrano* Fellowship. D.C. acknowledges the support of the Clore Scholars Programme and the Clore Israel Foundation. J.C.



acknowledges support from grant PID2021-124965NB-C22 funded by MICIU/AEI/10.13039/501100011033 and by “ERDF/EU”, European Union project C-QuENS (Grant No. 101135359), and grant CNS2023-144994 funded by MICIU/AEI/10.13039/501100011033 and by “ERDF/EU”.

- 
- [1] J.-H. Ardenkjaer-Larsen, G. S. Boebinger, A. Comment, S. Duckett, A. S. Edison, F. Engelke, C. Griesinger, R. G. Griffin, C. Hilty, H. Maeda, G. Parigi, T. Prisner, E. Ravera, J. van Bentum, S. Vega, A. Webb, C. Luchinat, H. Schwalbe, and L. Frydman, Facing and overcoming sensitivity challenges in biomolecular nmr spectroscopy, *Angewandte Chemie International Edition* **54**, 9162 (2015).
  - [2] D. L. Olson, T. L. Peck, A. G. Webb, R. L. Magin, and J. V. Sweedler, High-resolution microcoil  $^1\text{H}$ -nmr for mass-limited, nanoliter-volume samples, *Science* **270**, 1967 (1995).
  - [3] D. L. Olson, J. A. Norcross, M. O’Neil-Johnson, P. F. Molitor, D. J. Detlefsen, A. G. Wilson, and T. L. Peck, Microflow nmr: concepts and capabilities, *Analytical Chemistry* **76**, 2966 (2004).
  - [4] C. L. Degen, F. Reinhard, and P. Cappellaro, Quantum sensing, *Rev. Mod. Phys.* **89**, 035002 (2017).
  - [5] V. Giovannetti, S. Lloyd, and L. Maccone, Advances in quantum metrology, *Nature Photonics* **5**, 222 (2011).
  - [6] V. Giovannetti, S. Lloyd, and L. Maccone, Quantum metrology, *Phys. Rev. Lett.* **96**, 010401 (2006).
  - [7] J. M. Taylor, P. Cappellaro, L. Childress, L. Jiang, D. Budker, P. R. Hemmer, A. Yacoby, R. Walsworth, and M. D. Lukin, High-sensitivity diamond magnetometer with nanoscale resolution, *Nature Physics* **4**, 810 (2008).
  - [8] A. Ermakova, G. Pramanik, J.-M. Cai, G. Algara-Siller, U. Kaiser, T. Weil, Y.-K. Tzeng, H. C. Chang, L. P. McGuinness, M. B. Plenio, B. Naydenov, and F. Jelezko, Detection of a few metallo-protein molecules using color centers in nanodiamonds, *Nano Letters* **13**, 3305 (2013).
  - [9] H. J. Mamin, M. Kim, M. H. Sherwood, C. T. Rettner, K. Ohno, D. D. Awschalom, and D. Rugar, Nanoscale nuclear magnetic resonance with a nitrogen-vacancy spin sensor, *Science* **339**, 557 (2013).
  - [10] C. Müller, X. Kong, J.-M. Cai, K. Melentijevic, A. Stacey, M. Markham, D. Twitchen, J. Isoya, S. Pezzagna, J. Meijer, J. F. Du, M. B. Plenio, B. Naydenov, L. P. McGuinness, and F. Jelezko, Nuclear magnetic resonance spectroscopy with single spin sensitivity, *Nature Communications* **5**, 4703 (2014).
  - [11] A. Ajoy, U. Bissbort, M. D. Lukin, R. L. Walsworth, and P. Cappellaro, Atomic-scale nuclear spin imaging using quantum-assisted sensors in diamond, *Phys. Rev. X* **5**, 011001 (2015).
  - [12] I. Lovchinsky, A. O. Sushkov, E. Urbach, N. P. de Leon, S. Choi, K. De Greve, R. Evans, R. Gertner, E. Bersin, C. Müller, L. McGuinness, F. Jelezko, R. L. Walsworth, H. Park, and M. D. Lukin, Nuclear magnetic resonance detection and spectroscopy of single proteins using quantum logic, *Science* **351**, 836 (2016).
  - [13] D. R. Glenn, D. B. Bucher, J. Lee, M. D. Lukin, H. Park, and R. L. Walsworth, High-resolution magnetic resonance spectroscopy using a solid-state spin sensor, *Nature* **555**, 351 (2018).
  - [14] P. Wang, S. Chen, M. Guo, S. Peng, M. Wang, M. Chen, W. Ma, R. Zhang, J. Su, X. Rong, F. Shi, T. Xu, and J. Du, Nanoscale magnetic imaging of ferritins in a single cell, *Science Advances* **5**, eaau8038 (2019).
  - [15] J. Barton, M. Gulka, J. Tarabek, Y. Mindarava, Z. Wang, J. Schimer, H. Raabova, J. Bednar, M. B. Plenio, F. Jelezko, M. Nesladek, and P. Cigler, Nanoscale dynamic readout of a chemical redox process using radicals coupled with nitrogen-vacancy centers in nanodiamonds, *ACS Nano* **14**, 12938 (2020).
  - [16] C. L. Degen, M. Poggio, H. J. Mamin, and D. Rugar, Role of spin noise in the detection of nanoscale ensembles of nuclear spins, *Phys. Rev. Lett.* **99**, 250601 (2007).
  - [17] F. Reinhard, F. Shi, N. Zhao, F. Rempp, B. Naydenov, J. Meijer, L. T. Hall, L. Hollenberg, J. Du, R.-B. Liu, and J. Wrachtrup, Tuning a spin bath through the quantum-classical transition, *Phys. Rev. Lett.* **108**, 200402 (2012).
  - [18] B. E. Herzog, D. Cadeddu, F. Xue, P. Peddibhotla, and M. Poggio, Boundary between the thermal and statistical polarization regimes in a nuclear spin ensemble, *Applied Physics Letters* **105**, 043112 (2014).
  - [19] L. Viola, E. Knill, and S. Lloyd, Dynamical decoupling of open quantum systems, *Phys. Rev. Lett.* **82**, 2417 (1999).
  - [20] L. Cywiński, R. M. Lutchyn, C. P. Nave, and S. Das Sarma, How to enhance dephasing time in superconducting qubits, *Phys. Rev. B* **77**, 174509 (2008).
  - [21] C. A. Ryan, J. S. Hodges, and D. G. Cory, Robust decoupling techniques to extend quantum coherence in diamond, *Phys. Rev. Lett.* **105**, 200402 (2010).
  - [22] D. Cohen, T. Gefen, L. Ortiz, and A. Retzker, Achieving the ultimate precision limit with a weakly interacting quantum probe, *npj Quantum Information* **6**, 83 (2020).
  - [23] P. P. Mitra, P. N. Sen, L. M. Schwartz, and P. Le Doussal, Diffusion propagator as a probe of the structure of porous media, *Phys. Rev. Lett.* **68**, 3555 (1992).
  - [24] G. A. Álvarez and D. Suter, Measuring the spectrum of colored noise by dynamical decoupling, *Phys. Rev. Lett.* **107**, 230501 (2011).
  - [25] D. Cohen, R. Nigmatullin, M. Eldar, and A. Retzker, Confined nano-nmr spectroscopy using nv centers, *Advanced Quantum Technologies* **n/a**, 2000019 (2020).
  - [26] K. S. Liu, X. Ma, R. Rizzato, A. L. Semrau, A. Henning, I. D. Sharp, R. A. Fischer, and D. B. Bucher, Using metal-organic frameworks to confine liquid samples for nanoscale nv-nmr, *Nano Letters* **22**, 9876 (2022).
  - [27] P. S. Hubbard, Nuclear magnetic relaxation by intermolecular dipole-dipole interactions, *Phys. Rev.* **131**, 275 (1963).

- [28] T. Staudacher, N. Raatz, S. Pezzagna, J. Meijer, F. Reinhard, C. A. Meriles, and J. Wrachtrup, Probing molecular dynamics at the nanoscale via an individual paramagnetic centre, *Nature Communications* **6**, 8527 (2015).
- [29] K. S. Liu, A. Henning, M. W. Heindla, R. D. Allert, J. D. Bartla, I. D. Sharp, R. Rizzato, and D. B. Bucher, Surface nmr using quantum sensors in diamond, *Proceedings of the National Academy of Sciences* **120**, 12345 (2023).
- [30] N. Staudenmaier, A. Vijayakumar-Sreeja, G. Genov, D. Cohen, C. Findler, J. Lang, A. Retzker, F. Jelezko, and S. Oviedo-Casado, Optimal sensing protocol for statistically polarized nano-nmr with nv centers, *Phys. Rev. Lett.* **131**, 150801 (2023).
- [31] D. Cohen, R. Nigmatullin, O. Kenneth, F. Jelezko, M. Khodas, and A. Retzker, Utilising nv based quantum sensing for velocimetry at the nanoscale, *Scientific Reports* **10**, 5298 (2020).
- [32] A. Fick, V. on liquid diffusion, *The London, Edinburgh, and Dublin Philosophical Magazine and Journal of Science* **10**, 30 (1855).
- [33] J. Kuldová, F. Uhlík, and P. Košován, The drag of the tails: Diffusion of sticky nanoparticles in dilute polymer solutions, *The Journal of Chemical Physics* **143**, 243129 (2015).
- [34] S. Ray, Space-dependent diffusion with stochastic resetting: A first-passage study, *The Journal of Chemical Physics* **153**, 234904 (2020).
- [35] U. Boehm, S. Cox, G. Gantner, and R. Stevenson, Fast solutions for the first-passage distribution of diffusion models with space-time-dependent drift functions and time-dependent boundaries, *Journal of Mathematical Psychology* **105**, 102613 (2021).
- [36] A. Alexandre, M. Mangeat, T. Guérin, and D. S. Dean, How stickiness can speed up diffusion in confined systems, *Phys. Rev. Lett.* **128**, 210601 (2022).
- [37] A. Vilquin, V. Bertin, E. Raphaël, D. S. Dean, T. Salez, and J. D. McGraw, Nanoparticle taylor dispersion near charged surfaces with an open boundary, *Phys. Rev. Lett.* **130**, 038201 (2023).
- [38] T. R. Gentile, P. J. Nacher, B. Saam, and T. G. Walker, Optically polarized  $^3\text{He}$ , *Rev. Mod. Phys.* **89**, 045004 (2017).
- [39] K. Roger, E. Sparr, and H. Wennerström, Evaporation, diffusion and self-assembly at drying interfaces, *Phys. Chem. Chem. Phys.* **20**, 10430 (2018).
- [40] N. Staudenmaier, A. Vijayakumar-Sreeja, S. Oviedo-Casado, G. Genov, D. Cohen, D. Dulog, T. Unden, N. Striegler, A. Marshall, J. Scheuer, C. Findler, J. Lang, I. Schwartz, P. Neumann, A. Retzker, and F. Jelezko, Power-law scaling of correlations in statistically polarised nano-nmr, *npj Quantum Information* **8**, 120 (2022).
- [41] L. M. Pham, S. J. DeVience, F. Casola, I. Lovchinsky, A. O. Sushkov, E. Bersin, J. Lee, E. Urbach, P. Cappellaro, H. Park, A. Yacoby, M. Lukin, and R. L. Walsworth, Nmr technique for determining the depth of shallow nitrogen-vacancy centers in diamond, *Phys. Rev. B* **93**, 045425 (2016).
- [42] S. Oviedo-Casado, A. Rotem, R. Nigmatullin, J. Prior, and A. Retzker, Correlated noise in brownian motion allows for super resolution, *Scientific Reports* **10**, 19691 (2020).
- [43] J. M. Boss, K. S. Cujia, J. Zopes, and C. L. Degen, Quantum sensing with arbitrary frequency resolution, *Science* **356**, 837 (2017).
- [44] S. Schmitt, T. Gefen, F. M. Stürner, T. Unden, G. Wolff, C. Müller, J. Scheuer, B. Naydenov, M. Markham, S. Pezzagna, J. Meijer, I. Schwarz, M. Plenio, A. Retzker, L. P. McGuinness, and F. Jelezko, Submillihertz magnetic spectroscopy performed with a nanoscale quantum sensor, *Science* **356**, 832 (2017).
- [45] N. Staudenmaier, A. Vijayakumar-Sreeja, G. Genov, D. Cohen, C. Findler, J. Lang, A. Retzker, F. Jelezko, and S. Oviedo-Casado, Optimal sensing protocol for statistically polarized nano-nmr with nv centers, *Phys. Rev. Lett.* **131**, 150801 (2023).
- [46] T. Gefen, F. Jelezko, and A. Retzker, Control methods for improved fisher information with quantum sensing, *Phys. Rev. A* **96**, 032310 (2017).
- [47] Z. Li, X. Kong, H. Sun, G. Qu, P. Yu, T. Xie, Z. Zhao, G. Shi, Y. Wang, F. Shi, and J. Du, *Discovery of an anomalous non-evaporating sub-nanometre water layer in open environment* (2024), arXiv:2412.17636 [cond-mat.mtrl-sci].
- [48] W. Zheng, S. Zhang, J. Jiang, Y. He, R. Stöhr, A. Denisenko, J. Wrachtrup, X. C. Zeng, K. Bian, E.-G. Wang, and Y. Jiang, *Observation of liquid-solid transition of nanoconfined water at ambient temperature* (2024), arXiv:2412.15001 [cond-mat.mes-hall].
- [49] D. Pagliero, R. Khan, K. Elkaduwe, A. Bhardwaj, K. Xu, A. Wolcott, G. López, B. Radha, N. Giovambattista, and C. A. Meriles, *Slow water in engineered nano-channels revealed by color-center-enabled sensing* (2024), arXiv:2412.18969 [cond-mat.mes-hall].
- [50] E. Heifetz and S. Zucker, Fluid-like representation of Fickian diffusion, *Physics of Fluids* **34**, 011701 (2022).
- [51] S. Chanda and G. Natarajan, *comment on “fluid-like representation of fickian diffusion”* [phys. fluids 34, 011701 (2022)]<sub>i/p</sub>, *Physics of Fluids* **34**, 049101 (2022).
- [52] S. Oviedo-Casado, J. Prior, and J. Cerrillo, Low frequency signal detection via correlated ramsey measurements, *Journal of Magnetic Resonance* **363**, 107691 (2024).

## Appendix A: Diffusion on a cylinder with sticky walls

We aim to calculate the correlation function (in the time domain) for statistically polarized diffusing nuclei. Details on the derivation of the dephasing effect of the magnetic field produced by the nuclei at the NV center position given a specific control protocol, and how to derive expressions to calculate the corresponding correlation function can be found in the Supplemental Materials of [31] and [25]. In this Appendix we focus on the derivation of the correlation function for sticky walls.

The generic correlation function in the time domain reads

$$G^{m_1, m_2}(t) \propto \int \int f^{m_1 *}(\bar{r}) f^{m_2}(\bar{r}_0) P(\bar{r}, t | \bar{r}_0, t = 0) d^3 r d^3 r_0, \quad (\text{A1})$$

where the  $f^{m_i}$  are the spatial dependencies of the respective magnetic fields generated by each of the two nuclei. Using the polar symmetry of the problem, given that we want to measure the correlations at the NV position, and assuming that the NV is oriented in the  $z$  direction,  $f^{m_i} = Y_2^{m_i}(\Omega)/r^3$  with  $m = 0, 1, 2$ . Each of these components can be probed separately, yielding similar results (i.e. equal functional form up to a numerical factor). Therefore, throughout, we focus on the  $m = 0$  component and drop the superscript, for which

$$Y_2^0(\Omega) = \frac{4\sqrt{\pi}}{\sqrt{5}}(3 \cdot \cos^2 \theta - 1) = \frac{4\sqrt{\pi}}{\sqrt{5}} \left( \frac{3z^2}{r^2} - 1 \right) = \frac{4\sqrt{\pi}}{\sqrt{5}} \left[ \frac{3z^2}{(z^2 + \rho^2)} - 1 \right]. \quad (\text{A2})$$

$P(r, t | r_0, t = 0)$  in Eq. (A1) represents the nuclei propagator from point  $\bar{r}_0$  to  $\bar{r}$  in a time  $t$ . This propagator is the solution to a diffusion equation. Then, the first step is to solve that equation.

In this article, we consider free Fickian diffusion without drift for the liquid sample, which corresponds to the motion of pressureless, compressible Navier-Stokes equations or, alternatively, to isothermal Navier-Stokes motion due to concentration gradients of an irrotational fluid [50, 51]. The diffusion equation in three dimensions reads

$$\frac{\partial P}{\partial t} = D \nabla^2 P, \quad (\text{A3})$$

with  $D$  the (constant) diffusion coefficient. For uniform initial conditions  $P(\bar{r}, t = 0 | \bar{r}_0, t = 0) = \delta(\bar{r} - \bar{r}_0)$ , this equation is fulfilled in the whole space by the propagator

$$P(\bar{r}, t | \bar{r}_0, t = 0) = \frac{1}{(4\pi Dt)^{\frac{3}{2}}} \exp \left[ -\frac{(\bar{r} - \bar{r}_0)^2}{4Dt} \right]. \quad (\text{A4})$$

In the sticky scenario we want to solve  $G(t)$  with the propagator Eq. (A4), considering that the NV center probe is located at a depth  $d$ . Moreover, we want to separate the correlation calculation in two distinct regions. The first one is the contribution from the nuclei on the inside of a cylinder of radius  $R$  and height  $L$ , with the vertical axis  $L$  coincident with the  $z$  axis and (perfectly) aligned with the NV center. The second is the contribution from the nuclei that have a fixed position on the boundaries of said cylinder, having diffused there.

For the propagator Eq. (A4) the correlation function reads

$$G^{\text{sticky}}(t) = \frac{\Upsilon \sqrt{\pi}}{2(Dt)^{\frac{3}{2}}} \int \int \frac{Y_2^{0*}(\Omega)}{r^3} \frac{Y_2^0(\Omega_0)}{r_0^3} \exp \left[ -\frac{(\bar{r} - \bar{r}_0)^2}{4Dt} \right] d^3 r d^3 r_0, \quad (\text{A5})$$

with  $\Upsilon$  the nuclear spin density, which we take as  $\Upsilon = 1$ . The task is to solve this integral. Transforming the exponential to cylindrical coordinates we have that

$$G^{\text{sticky}}(t) = \frac{\sqrt{\pi}}{2(Dt)^{\frac{3}{2}}} \int \int \frac{Y_2^{0*}(\Omega)}{r^3} \frac{Y_2^0(\Omega_0)}{r_0^3} \exp \left[ -\frac{(\bar{\rho} - \bar{\rho}_0)^2}{4Dt} \right] \exp \left[ -\frac{(z - z_0)^2}{4Dt} \right] d^3 r d^3 r_0, \quad (\text{A6})$$

with  $\bar{\rho}$  the position in polar coordinates  $(\rho, \phi)$ . Here the problem is that  $\Omega$  is the solid angle in spherical coordinates, while  $\bar{\rho}$  involves the polar angle only. Note that  $r^2 = \rho^2 + z^2$ .

The first step is to try an get rid of the angles in the integral of  $G^{\text{sticky}}(t)$ . To do so, we inverse Fourier transform the Gaussian containing  $\bar{\rho} - \bar{\rho}_0$ , which is an inverse 2D Fourier transform on the plane. This yields

$$G^{\text{sticky}}(t) = \frac{1}{8\pi^2(\pi Dt)^{\frac{1}{2}}} \int \int \int \frac{Y_2^{0*}(\Omega)}{r^3} \frac{Y_2^0(\Omega_0)}{r_0^3} \exp(-Dtk^2) \exp(-i\bar{k} \cdot \bar{\rho} + i\bar{k} \cdot \bar{\rho}_0) \exp \left[ -\frac{(z - z_0)^2}{4Dt} \right] d^3 r d^3 r_0 d^2 k. \quad (\text{A7})$$

To resolve the scalar product  $\bar{k} \cdot \bar{r}$  we use the Anger-Jacobi expansion

$$\exp(-i\bar{k} \cdot \bar{r}) = \exp(-ikr \cos \chi) = \sum_{n=-\infty}^{\infty} i^n \exp(in\chi) J_n(kr), \quad (\text{A8})$$

which applied to  $G^{\text{sticky}}(t)$  yields

$$G^{\text{sticky}}(t) = \frac{n}{8\pi^2(\pi Dt)^{\frac{1}{2}}} \sum_{n_1, n_2} \int \int \int \frac{Y_2^{0*}(\Omega) Y_2^0(\Omega_0)}{r^3 r_0^3} i^{n_1} (-i)^{n_2} \exp[i(n_1\chi - n_2\chi_0)] J_{n_1}(k\rho) J_{n_2}(k\rho_0) \exp(-Dtk^2) \exp\left[-\frac{(z-z_0)^2}{4Dt}\right] d^3r d^3r_0 d^2k, \quad (\text{A9})$$

with  $\chi$  ( $\chi_0$ ) the angle between  $\bar{k}$  and  $\bar{r}$  ( $\bar{r}_0$ ).

The angles  $\{\chi, \chi_0\}$  are related to  $\{\phi, \phi_0\}$  via the free angle of  $\bar{k}$ , such that  $\chi = \chi' - \phi$  and  $\chi_0 = \chi' - \phi_0$ . Then, we can then get rid of  $\phi, \phi_0$  by using the expression for the spherical harmonics and integrating. Since we have chosen  $m = 0$ , and  $\phi$  goes from 0 to  $2\pi$ , this is the definition of scalar product for the spherical harmonics, and then only the integrals with  $n_1$  or  $n_2 = m$  survive, meaning that we get

$$G^{\text{sticky}}(t) = \sqrt{\frac{\pi}{Dt}} \int \int \int \frac{Y_2^{0*}(\theta) Y_2^0(\theta_0)}{r^3 r_0^3} J_0(k\rho) J_0(k\rho_0) \exp(-Dtk^2) \exp\left[-\frac{(z-z_0)^2}{4Dt}\right] kd^2r d^2r_0 dk. \quad (\text{A10})$$

We want to integrate this in two different regions. The first one, with  $\rho, \rho_0 \in \{0, R\}$  and  $z, z_0 \in \{d, d+L\}$ , and the second  $\rho \in \{R, \infty\}$ ,  $z \in \{d+L, \infty\}$ ,  $\rho_0 \in \{0, R\}$ ,  $z_0 \in \{d, d+L\}$ . To get rid of  $\theta$ , we convert the spherical harmonics and  $r$  to  $\rho, z$  coordinates.

We will have to solve the integrals numerically, but we want to try and get rid of as many variables as we can analytically. The most obvious simplification is the integral in the moments  $k$ . We then solve first this integral using the following identity for the Bessel functions:

$$\int_0^\infty x \exp(-px^2) J_m(ax) J_m(bx) dx = \frac{\exp\left(\frac{-a^2-b^2}{4p}\right)}{2p} I_m\left(\frac{ab}{2p}\right), \quad (\text{A11})$$

that yields

$$\int_0^\infty k J_m(k\rho) J_m(k\rho_0) \exp(-Dtk^2) dk = \frac{1}{2Dt} \exp\left(\frac{-\rho^2 - \rho_0^2}{4Dt}\right) I_m\left(\frac{\rho\rho_0}{2Dt}\right), \quad (\text{A12})$$

which when applied back to Eq. (A10) gives us the most simplified expression possible to solve numerically:

$$G^{\text{sticky}}(t) = \frac{\sqrt{\pi}}{2(Dt)^{\frac{3}{2}}} \int \int \int \int d\rho d\rho_0 dz dz_0 \rho \rho_0 I_0\left(\frac{\rho\rho_0}{2Dt}\right) \left[ \frac{3z^2}{(\rho^2 + z^2)^{5/2}} - \frac{1}{(\rho^2 + z^2)^{3/2}} \right] \left[ \frac{3z_0^2}{(\rho_0^2 + z_0^2)^{5/2}} - \frac{1}{(\rho_0^2 + z_0^2)^{3/2}} \right] \exp\left(\frac{-\rho^2 - \rho_0^2}{4Dt}\right) \exp\left[-\frac{(z-z_0)^2}{4Dt}\right]. \quad (\text{A13})$$

Let us now write explicitly, in each space domain, which integrals we have to solve:

### 1. Region $\rho, \rho_0 \in \{0, R\}$ and $z, z_0 \in \{d, d+L\}$

In this case we have,

$$G_{\text{bulk}}^{\text{sticky}}(t) = \frac{\sqrt{\pi}}{2(Dt)^{3/2}} \int_0^R d\rho \int_0^R d\rho_0 \int_d^{d+L} dz \int_d^{d+L} dz_0 \left[ \frac{3z^2}{(\rho^2 + z^2)^{5/2}} - \frac{1}{(\rho^2 + z^2)^{3/2}} \right] \left[ \frac{3z_0^2}{(\rho_0^2 + z_0^2)^{5/2}} - \frac{1}{(\rho_0^2 + z_0^2)^{3/2}} \right] \rho \rho_0 \exp\left[-\frac{(z-z_0)^2}{4Dt}\right] \exp\left(\frac{-\rho^2 - \rho_0^2}{4Dt}\right) I_0\left(\frac{\rho\rho_0}{2Dt}\right). \quad (\text{A14})$$

which is Eq.(6) on the main text.

**2. Region: cylinder surface, with  $\rho = R$  and  $z \in \{d+L, \infty\}$ ,  $z = d$  and  $\rho \in \{0, R\}$ ,  $z = d+L$  and  $\rho \in \{0, R\}$ , with  $\rho_0 \in \{0, R\}$  and  $z_0 \in \{d, d+L\}$**

In this case, we are interested in considering the nuclei that diffuse out of the cylinder region as getting glued to the walls on the exit point. Then, the initial condition for the propagator is still  $\rho_0 \in \{0, R\}$  and  $z_0 \in \{d, d+L\}$ , with the corresponding form factor  $f^0(\vec{r}_0)$  integrated also in these limits. In principle, we should integrate  $\{\rho, z\}$  on the outer region of the cylinder, but this implies solving numerically integrals that have an infinite upper limit. Rather, it is simpler to calculate the particles density remaining inside of the cylinder as a function of time, which corresponds to the propagator Eq. (A4) integrated on the first region

$$\zeta_{\text{bulk}}^{\text{sticky}}(t) = \frac{\sqrt{\pi}}{2V(Dt)^{\frac{3}{2}}} \int_0^R d\rho \int_0^R d\rho_0 \int_d^{d+L} dz \int_d^{d+L} dz_0 \rho \rho_0 I_0\left(\frac{\rho \rho_0}{2Dt}\right) \exp\left(\frac{-\rho^2 - \rho_0^2}{4Dt}\right) \exp\left[-\frac{(z - z_0)^2}{4Dt}\right], \quad (\text{A15})$$

and then obtain the density of nuclei that has already left the cylinder, using the conservation of particles, as  $1 - \zeta_{\text{bulk}}^{\text{sticky}}(t)$ .

To calculate the contribution to the overall correlation from these nuclei that have already reached the cylinder walls, we consider an initial uniform distribution on the bulk of the cylinder and an asymptotic infinite time distribution of the same nuclei on the surface, where the propagator becomes  $1/S$  the cylinder surface. Then, the contribution is calculated as

$$G^{\text{sticky}}(t \gg \tau_V) = \frac{4\pi^2}{S} \left\{ \int_0^R d\rho \rho \left[ \frac{3d^2}{(\rho^2 + d^2)^{5/2}} - \frac{1}{(\rho^2 + d^2)^{3/2}} \right] + \int_0^R d\rho \rho \left[ \frac{3(d+L)^2}{(\rho^2 + (d+L)^2)^{5/2}} - \frac{1}{(\rho^2 + (d+L)^2)^{3/2}} \right] \right. \\ \left. + \int_d^{d+L} dz R \left[ \frac{3z^2}{(R^2 + z^2)^{5/2}} - \frac{1}{(R^2 + z^2)^{3/2}} \right] \right\} \int_0^R d\rho_0 \int_d^{d+L} dz_0 \rho_0 \left[ \frac{3z_0^2}{(\rho_0^2 + z_0^2)^{5/2}} - \frac{1}{(\rho_0^2 + z_0^2)^{3/2}} \right], \quad (\text{A16})$$

which results in

$$G^{\text{sticky}}(t \gg \tau_V) = \frac{2\pi}{R+L} \left[ \frac{d}{\sqrt{(d+L)^2 + R^2}} - \frac{d}{\sqrt{d^2 + R^2}} + \frac{L}{\sqrt{(d+L)^2 + R^2}} \right] \left\{ \frac{R}{(d^2 + R^2)^{3/2}} + \frac{R}{((d+L)^2 + R^2)^{3/2}} - \right. \\ \left. \frac{d^2 L (\sqrt{d^2 + R^2} - 2\sqrt{(d+L)^2 + R^2}) + dR^2 (\sqrt{d^2 + R^2} - \sqrt{(d+L)^2 + R^2}) + LR^2 \sqrt{d^2 + R^2} + d^3 (\sqrt{d^2 + R^2} - \sqrt{(d+L)^2 + R^2}) - dL^2 \sqrt{(d+L)^2 + R^2}}{[(d^2 + R^2)((d+L)^2 + R^2)]^{3/2}} \right\}. \quad (\text{A17})$$

The contribution to the overall correlation by the nuclei in the walls of the cylinder is then  $G^{\text{sticky}}(t \gg \tau_V)[1 - \zeta_{\text{bulk}}^{\text{sticky}}(t)]$ .

### 3. Initial correlation signal amplitude or $B_{\text{rms}}^2$

For completeness, note that the  $B_{\text{rms}}$  corresponds to an initial uniform distribution on the cylinder volume, and it is therefore calculated as

$$G(t=0) = B_{\text{rms}}^2 = \frac{16\pi}{5} \int_0^R d\rho \int_d^{d+L} dz \rho^2 \left[ \frac{3z^2}{(\rho^2 + z^2)^{5/2}} - \frac{1}{(\rho^2 + z^2)^{3/2}} \right]^2. \quad (\text{A18})$$

## Appendix B: Diffusion in a cylinder with constant evaporation on the boundaries

In this section, we solve the diffusion equation inside a cylinder region enclosed by walls that allow evaporation on their surface, reflected as boundary conditions. Working in cylindrical coordinates we have that the diffusion equation reads

$$\frac{dP}{dt} - D \left[ \frac{1}{\rho} \frac{d}{d\rho} \left( \rho \frac{dP}{d\rho} \right) + \frac{1}{\rho^2} \frac{d^2 P}{d\phi^2} + \frac{d^2 P}{dz^2} \right] = 0 \quad (\text{B1})$$

with boundary conditions

$$\left( \frac{dP}{d\rho} + \frac{d}{D\tau_{\text{ev}}} P \right) \Big|_{\rho=R} = 0 \quad \left( \frac{dP}{dz} - \frac{d}{D\tau_{\text{ev}}} P \right) \Big|_{z=d} = 0 \quad \left( \frac{dP}{dz} + \frac{d}{D\tau_{\text{ev}}} P \right) \Big|_{z=d+L} = 0 \quad P(\phi + 2\pi) = P(\phi), \quad (\text{B2})$$

where  $d$  represents the NV-depth, and we define  $\tau_{\text{ev}}$  as the characteristic time at which outward diffusion takes place on the boundaries, that is, the time it takes to decrease the initial concentration by  $1/e$ . The initial condition is the uniform distribution

$$P(\rho, \phi, z, t = 0) = \frac{1}{\rho} \delta(\rho - \rho_0) \delta(z - z_0) \delta(\phi - \phi_0). \quad (\text{B3})$$

We try to solve this equation by the method of separation of variables. As a first step, we consider a solution of the form  $P = T(t)f(\rho, \phi, z)$ . Then, the diffusion equation is

$$\frac{1}{DT} \frac{dT}{dt} = -\lambda^2 = \frac{1}{\rho f} \left[ \frac{d}{d\rho} \left( \rho \frac{df}{d\rho} \right) + \frac{1}{\rho^2} \frac{d^2 f}{d\phi^2} + \frac{d^2 f}{dz^2} \right], \quad (\text{B4})$$

from where we get  $T(t) = A_T \exp(-D\lambda^2 t)$ . The eigenvalues  $\lambda \in \mathbb{R}$  are chosen to yield modes that can only decay with time. The value  $\lambda = 0$  leads to just a trivial solution for the given boundary condition, which does not decay and would simply recover the perfectly reflective walls limit [25]. Therefore, we disregard it. The next step is to further separate the spatial variables as  $f(\rho, \phi, z) = Z(z)g(\rho, \phi)$ . Then

$$-\frac{1}{Z} \frac{d^2 Z}{dz^2} = \pm \eta^2 = \frac{1}{g} \left[ \frac{d}{d\rho} \left( \rho \frac{dg}{d\rho} \right) + \frac{1}{\rho^2} \frac{d^2 g}{d\phi^2} + \lambda^2 g \right], \quad (\text{B5})$$

where we assumed that  $\eta \in \mathbb{R}$ . For  $Z(z)$  we have a second order differential equation of the harmonic oscillator family, with the following boundary conditions:

$$\frac{d^2 Z(z)}{dz^2} \pm \eta^2 Z(z) = 0 \quad \left[ \frac{dZ(z)}{dz} - \frac{d}{D\tau_{\text{ev}}} Z(z) \right]_{z=d} = 0 \quad \left[ \frac{dZ(z)}{dz} + \frac{d}{D\tau_{\text{ev}}} Z(z) \right]_{z=d+L} = 0. \quad (\text{B6})$$

Considering the two possible signs for the eigenvalues,  $Z(z)$  can be either  $Z(z) = C_2 \sin[\eta(z-d)] + C_3 \cos[\eta(z-d)]$  or  $Z(z) = C_2^h \sinh[\eta(z-d)] + C_3^h \cosh[\eta(z-d)]$ . Beginning with the solution involving trigonometric functions, and applying the boundary conditions, we get that

$$\begin{aligned} \eta C_2 - \frac{d}{D\tau_{\text{ev}}} C_3 &= 0 \\ (\eta C_2 + \frac{d}{D\tau_{\text{ev}}} C_3) \cos(\eta L) + (\frac{d}{D\tau_{\text{ev}}} C_2 - \eta C_3) \sin(\eta L) &= 0. \end{aligned} \quad (\text{B7})$$

These equations can be satisfied choosing  $\eta_m$  to be the solutions to the transcendental equation

$$\tan(\eta L) = \frac{2d\eta}{d^2 - \eta^2 D^2 \tau_{\text{ev}}^2}, \quad (\text{B8})$$

yielding

$$Z(z) = C_m \left( \sin[\eta_m(z-d)] + \frac{\eta_m D\tau_{\text{ev}}}{d} \cos[\eta_m(z-d)] \right). \quad (\text{B9})$$

Note that  $\eta = 0$  leaves  $C_m$  undetermined.

Another option to satisfy the boundary conditions is to try to nullify both cosine and sine coefficients, that is

$$\eta C_2 - \frac{d}{D\tau_{\text{ev}}} C_3 = 0, \quad (\text{B10})$$

$$\eta C_2 + \frac{d}{D\tau_{\text{ev}}} C_3 = 0, \quad (\text{B11})$$

$$\frac{d}{D\tau_{\text{ev}}} C_2 - \eta C_3 = 0, \quad (\text{B12})$$

$$(\text{B13})$$

which can only be satisfied if  $\eta = 0$ . Before assigning an eigenfunction to  $\eta = 0$  let us consider the alternative solution for  $Z(z)$ .



Considering now  $Z(z)$  with hyperbolic functions, the boundary conditions read

$$\begin{aligned} \eta C_2 - \frac{d}{D\tau_{\text{ev}}} C_3 &= 0 \\ \left( \eta C_2 + \frac{d}{D\tau_{\text{ev}}} C_3 \right) \cosh(\eta L) + \left( \frac{d}{D\tau_{\text{ev}}} C_2 + \eta C_3 \right) \sinh(\eta L) &= 0, \end{aligned} \quad (\text{B14})$$

which cannot be satisfied simultaneously unless  $\eta = 0$ . Then, for  $\eta = 0$ , we must have  $Z(z) = A_0 + B_0 z$  a constant, but such function cannot satisfy the boundary conditions unless  $A_0 = 0 = B_0$ , meaning that there is no  $\eta = 0$  eigenvalue, nor are hyperbolic functions a possible solution to the diffusion equation satisfying the evaporation boundary conditions. This leaves us with the trigonometric functions solutions.

To simplify the calculation, we can write the boundary conditions as harmonic functions that are rather centred at the horizontal symmetry plane at  $z = d + L/2$  of the cylinder:  $C_2 \sin \left[ \eta \left( z - d - \frac{L}{2} \right) \right] + C_3 \cos \left[ \eta \left( z - d - \frac{L}{2} \right) \right]$ , leading to the following equations from the boundary conditions

$$\left( \eta C_3 + \frac{d}{D\tau_{\text{ev}}} C_2 \right) \sin \left( \frac{\eta L}{2} \right) + \left( \eta C_2 - \frac{d}{D\tau_{\text{ev}}} C_3 \right) \cos \left( \frac{\eta L}{2} \right) = 0, \quad (\text{B15})$$

$$\left( -\eta C_3 + \frac{d}{D\tau_{\text{ev}}} C_2 \right) \sin \left( \frac{\eta L}{2} \right) + \left( \eta C_2 + \frac{d}{D\tau_{\text{ev}}} C_3 \right) \cos \left( \frac{\eta L}{2} \right) = 0. \quad (\text{B16})$$

Summing both equations we arrive at

$$C_2 \left[ \frac{d}{D\tau_{\text{ev}}} \sin \left( \frac{\eta L}{2} \right) + \eta \cos \left( \frac{\eta L}{2} \right) \right] = 0, \quad (\text{B17})$$

meaning, either (\*)  $C_2 = 0$  or (\*\*)  $\left[ \frac{d}{D\tau_{\text{ev}}} \sin \left( \frac{\eta L}{2} \right) + \eta \cos \left( \frac{\eta L}{2} \right) \right] = 0$  or both.

Taking either (\*) or (\*\*) we arrive at

$$C_3 \left[ \eta \sin \left( \frac{\eta L}{2} \right) - \frac{d}{D\tau_{\text{ev}}} \cos \left( \frac{\eta L}{2} \right) \right] = 0 \quad (\text{B18})$$

To get a non trivial solution we must have

$$C_2 = 0, \quad \frac{\eta_0}{\eta} = \tan \left( \frac{\eta L}{2} \right) \quad (\text{B19})$$

or

$$C_3 = 0, \quad -\frac{\eta}{\eta_0} = \tan \left( \frac{\eta L}{2} \right) \quad (\text{B20})$$

Since  $\tan(x)$  is periodic and divergent, both equations have a discrete infinite sets of solutions denoted by  $\eta_m^{(\pm)}$  by the sign in the equation and the reflection symmetry of the solution. The transcendental equations (B19), (B20) have a slightly easier form to solve numerically than Eq. (B8), so we use this form. As well, they make explicit the defined parity with respect to the center of the cylinder, as should be expected. The eigenfunction  $Z(z)$  corresponding to these updated form for the eigenvalues gets split in two, such that for Eq. (B19) we get

$$Z^+(z) = C_+ \cos \left[ \eta_m^+ \left( z - d - \frac{L}{2} \right) \right], \quad (\text{B21})$$

while Eq. (B20) implies

$$Z^-(z) = C_- \cos \left[ \eta_m^- \left( z - d - \frac{L}{2} \right) \right]. \quad (\text{B22})$$

Taking only the eigenvalues that lead to decaying modes  $-\eta^2$ , leaves us with the radial and angular parts of the problem, with differential equation

$$\frac{d}{d\rho} \left( \rho \frac{dg}{d\rho} \right) + \frac{1}{\rho^2} \frac{d^2 g}{d\phi^2} + (\lambda^2 - \eta^2)g = 0, \quad (\text{B23})$$

for which we can decompose  $g = R(\rho) \exp(-in\phi)$ , with  $n \in \mathcal{Z}$  due to the periodic boundary condition in  $\phi$ . Then

$$\rho^2 \frac{d^2 R}{d\rho^2} + \rho \frac{dR}{d\rho} + [(\lambda^2 - \eta^2) \rho^2 - n^2] R = 0 \quad (\text{B24})$$

We can set  $\beta^2 = \lambda^2 - \eta^2$ , then

$$\frac{d^2 R}{d\rho^2} + \frac{1}{\rho} \frac{dR}{d\rho} + \left( \beta^2 - \frac{n^2}{\rho^2} \right) R = 0 \quad (\text{B25})$$

which is the Bessel equation with solution  $R(\rho) = C_4 J_n(\beta\rho) + C_5 Y_n(\beta\rho)$ , where, since at  $r = 0$  the propagator should be finite, then  $C_5 = 0$ , yielding  $R(\rho) = C_4 J_n(\beta\rho)$ . If we apply the boundary condition we get

$$J'_n(\xi) + \frac{dR}{\xi D\tau_{\text{ev}}} J_n(\xi) = 0, \quad \xi = \beta R \quad (\text{B26})$$

whose solutions, for each  $n$ , are the eigenvalues, meaning that for each  $n$  there is a family  $p = 0, 1, 2, \dots$  of eigenvalues  $\beta_{n,p}$ .

We note that the solutions with  $\beta^2 \leq 0$  cannot satisfy the boundary condition - For  $\beta = 0$  we arrive at a power-law solution from free diffusion, and the boundary condition dictates  $n = -\frac{dR}{d\tau_{\text{ev}}}$ , which is generally not true. For  $\beta^2 < 0$  the solutions are the modified Bessel functions  $I_n(\beta r)$ , which are infinite at zero radius, which does not hold; then the only solution to the boundary condition would be  $\beta = 0$ , which contradicts our assumption  $\beta^2 < 0$ .

Choosing then  $(\lambda_{m,n,p}^\pm)^2 = \beta_{n,p}^2 + (\eta_m^\pm)^2$ ,  $m > 0$ , the propagator is

$$P(\rho, \phi, z, t) = \sum_{m=1}^{\infty} \sum_{n=-\infty}^{\infty} \sum_{p=0}^{\infty} J_n(\beta_{n,p}\rho) \exp(-in\phi) \left\{ A_{m,n,p}^- \sin \left[ \eta_m^- \left( z - d - \frac{L}{2} \right) \right] \exp(-D(\lambda_{m,n,p}^-)^2 t) \right. \\ \left. + A_{m,n,p}^+ \cos \left[ \eta_m^+ \left( z - d - \frac{L}{2} \right) \right] \exp(-D(\lambda_{m,n,p}^+)^2 t) \right\}, \quad (\text{B27})$$

where we define global  $A$  amplitudes which condense all  $C'$ s utilised in the above derivation. Applying the  $t = 0$  condition to concrete the amplitudes we get

$$\sum_{m=1}^{\infty} \sum_{n=-\infty}^{\infty} \sum_{p=0}^{\infty} J_n(\beta_{n,p}\rho) \exp(-in\phi) \left\{ A_{m,n,p}^- \sin \left[ \eta_m^- \left( z - d - \frac{L}{2} \right) \right] \right. \\ \left. + A_{m,n,p}^+ \cos \left[ \eta_m^+ \left( z - d - \frac{L}{2} \right) \right] \right\} = \frac{1}{\rho} \delta(\rho - \rho_0) \delta(z - z_0) \delta(\phi - \phi_0), \quad (\text{B28})$$

which decouples  $m$  from  $n$  and  $p$ . Then

$$\sum_{m=1}^{\infty} A_m^- \sin \left[ \eta_m^- \left( z - d - \frac{L}{2} \right) \right] + A_m^+ \cos \left[ \eta_m^+ \left( z - d - \frac{L}{2} \right) \right] = \delta(z - z_0), \quad (\text{B29})$$

multiplying on both sides by the eigenfunctions, integrating, and using the normalization condition for  $\eta_m$  we get

$$A_m^+ = \frac{2}{L} \frac{1}{1 + \text{sinc}(\eta_m^+ L)} \cos \left[ \eta_m^+ \left( z_0 - d - \frac{L}{2} \right) \right] \quad (\text{B30})$$

$$A_m^- = \frac{2}{L} \frac{1}{1 - \text{sinc}(\eta_m^- L)} \sin \left[ \eta_m^- \left( z_0 - d - \frac{L}{2} \right) \right]. \quad (\text{B31})$$

The remaining part of the  $t = 0$  condition is

$$\sum_{n=-\infty}^{\infty} \sum_{p=0}^{\infty} A_{n,p} J_n(\beta_{n,p}\rho) \exp(-in\phi) = \frac{1}{\rho} \delta(\rho - \rho_0) \delta(\phi - \phi_0), \quad (\text{B32})$$

where we can use the same procedure as for the  $z$  coordinate. In this case, the orthogonality of the Bessel functions is defined by the boundary conditions of the third kind, which impose a norm that yields

$$A_{n,p} = \frac{(\beta_{n,p} R)^2 J_n(\beta_{n,p} \rho_0) \exp(in\phi_0)}{\pi R^2 \left[ \left( \frac{dR}{D\tau_{\text{ev}}} \right)^2 + (\beta_{n,p} R)^2 - n^2 \right] J_n(\beta_{n,p} R)^2}. \quad (\text{B33})$$

This completes the derivation. Using again the definition of  $\eta_0 = d/D\tau_{ev}$ , the propagator is

$$P(\rho, \phi, z, t) = \frac{L}{V} \sum_{m=1}^{\infty} \sum_{n=-\infty}^{\infty} \sum_{p=0}^{\infty} \frac{2(\beta_{n,p}R)^2 J_n(\beta_{n,p}\rho_0)}{L \left[ (\eta_0^2 R^2 + (\beta_{n,p}R)^2 - n^2) J_n(\beta_{n,p}R)^2 \right]} \times \\ \left\{ \frac{\sin \left[ \eta_m^- \left( z_0 - d - \frac{L}{2} \right) \right]}{1 - \text{sinc}(\eta_m^- L)} \sin \left[ \eta_m^- \left( z - d - \frac{L}{2} \right) \right] + \frac{\cos \left[ \eta_m^+ \left( z_0 - d - \frac{L}{2} \right) \right]}{1 + \text{sinc}(\eta_m^+ L)} \cos \left[ \eta_m^+ \left( z - d - \frac{L}{2} \right) \right] \right\} \times \\ J_n(\beta_{n,p}\rho) \exp \left[ -in(\phi - \phi_0) - D(\beta_{n,p}^2 + \eta_m^2) t \right]. \quad (\text{B34})$$

### 1. Calculation of the auto-correlation

Assuming only one of the dipole-dipole interaction terms is on-resonance the auto-correlation reads,

$$G^{(k)}(t) = \int \frac{d^3 r}{r^3} \int \frac{d^3 r_0}{r_0^3} Y_2^{(k)}(\vec{r}_0) \left[ Y_2^{(k)}(\vec{r}) \right]^* P(\vec{r}, \vec{r}_0, t) \quad (\text{B35})$$

The angular integration over  $\phi$  and  $\phi_0$  yields  $(2\pi)^2 \delta_{k,n}$ , therefore, the auto-correlation can be written as

$$G^{(k)}(t) = \frac{8\pi^2 \Upsilon^2}{V} \sum_{m=1}^{\infty} \sum_{p=0}^{\infty} \frac{(\beta_{k,p}R)^2}{\left[ (\eta_0 R)^2 + (\beta_{k,p}R)^2 - k^2 \right] J_k^2(\beta_{k,p}R)} \exp \left( -\frac{t}{\tau_{k,m,p}} \right) \times \quad (\text{B36})$$

$$\left( \int_0^R d\rho \cdot \rho \int_d^{d+L} dz Y_2^{(k)}(z, \rho) J_k(\beta_{k,p}\rho) \left\{ \frac{\sin \left[ \eta_m^- \left( z_0 - d - \frac{L}{2} \right) \right]}{1 - \text{sinc}(\eta_m^- L)} \sin \left[ \eta_m^- \left( z - d - \frac{L}{2} \right) \right] + \right. \right. \quad (\text{B37})$$

$$\left. \frac{\cos \left[ \eta_m^+ \left( z_0 - d - \frac{L}{2} \right) \right]}{1 + \text{sinc}(\eta_m^+ L)} \cos \left[ \eta_m^+ \left( z - d - \frac{L}{2} \right) \right] \right\}^2 + \quad (\text{B38})$$

$$\frac{8\pi^2}{V} \sum_{p=p_0}^{\infty} \frac{\eta_0 L}{1 - e^{-2\eta_0 L}} \frac{(\beta_{k,p}R)^2}{\left[ (\eta_0 R)^2 + (\beta_{k,p}R)^2 - n^2 \right] J_k^2(\beta_{k,p}R)} \times \quad (\text{B39})$$

$$\left\{ \int_0^R d\rho \cdot \rho \int_d^{d+L} dz Y_2^{(k)}(z, \rho) J_k(\beta_{k,p}\rho) [\sinh(\eta_0(z-d)) - \cosh(\eta_0(z-d))] \right\}^2 \exp \left( -\frac{t}{\tau_{k,0,p}} \right), \quad (\text{B40})$$

where we have defined the decay coefficients as  $\tau_{m,p} = 1/D(\beta_p^2 + \eta_m^2)$ . In this article,  $k = 0$ , yielding Eq. (20).

### Appendix C: Decay modes for evaporating walls

We begin by estimating the value of  $\tau_{0,0}$  in the regime of  $\tau_{ev} \gg T_D$ . We note that  $\eta_0 = d/D\tau_{ev}$  and  $T_D = d^2/D$ , so  $\eta_0 d \ll 1$  which implies that, for moderate confining volumes,  $\eta_0 L, \eta_0 R \ll 1$ .  $\tau_{0,0}$  is a function of  $\beta_0$  and  $\eta_1^\pm$  so we begin by solving Eq. (15):

$$\xi J_0'(\xi) + (\eta_0 R) J_0(\xi) = 0. \quad (\text{C1})$$

In the limit  $\eta_0 R \ll 1$  the smallest solution to the equation should be close to the first zero of  $J_0'(\xi)$ , which is  $\xi = 0$ . Taking a series expansion near this point we have

$$\xi \left( -\frac{\xi}{2} \right) + (\eta_0 R) \left( 1 - \frac{\xi^2}{4} \right) \approx 0. \quad (\text{C2})$$

Hence, we find that

$$\xi = 2\sqrt{\frac{\eta_0 R}{2 + \eta_0 R}} \approx \sqrt{2\eta_0 R} \quad (\text{C3})$$

Now we turn our attention to Eq. (14),

$$\pm \frac{\eta_0}{\eta} = \tan\left(\frac{\eta L}{2}\right) \quad (\text{C4})$$

The decay is minimal for  $\eta L \ll 1$ , which leads to

$$\eta^2 = \frac{2\eta_0}{L} \quad (\text{C5})$$

Then,

$$\tau_{0,0} \approx \frac{1}{\eta_0 D} \left(\frac{1}{R} + \frac{1}{L}\right)^{-1} = \frac{\tau_{ev}}{d} \left(\frac{2}{R} + \frac{2}{L}\right)^{-1}. \quad (\text{C6})$$

Note, that  $\frac{S}{V} = \frac{2\pi R^2}{\pi R^2 L} + \frac{2\pi RL}{\pi R^2 L} = \frac{2}{L} + \frac{2}{R}$ , hence,

$$\tau_{0,0} \approx \frac{\tau_{ev}}{d} \frac{V}{S}, \quad (\text{C7})$$

as we use in Eq. (28).

We now calculate numerically the evaporation correlation function decay rates  $\tau_{m,p}^{+,-} = 1/D(\beta_p^2 + \eta_m^{+,-2})$ , for a wide variety of confinement region surface to volume  $S/V$  ratios and evaporation rates  $\tau_{ev}$ , and compare them to the main assumptions employed to obtain the simplified expression for the correlations Eq. (28), namely, that when  $\eta_0 L, \eta_0 R \ll 1$  the eigenvalue  $\tau_{0,0}^+$  is significantly dominant over all other eigenvalues, and that, in general,  $\tau_{0,0}^+ \approx V\tau_{ev}/Sd$ .

For all possible values of  $\tau_{ev}$ , radius and height of the confinement volume,  $\tau_{0,0}^+$  calculated with  $\eta_0^+$  is the greatest eigenvalue, that provides the fastest decay of the correlations. The second most important eigenvalue depends on the ratio between the radius  $R$  and the height  $L$ . Thus, if  $R > L$ , the secondary decay rate is given by  $\tau_{1,0}^+$ , while if  $L > R$  then the secondary decay rate is given by  $\tau_{0,0}^-$ , i.e. that with  $\eta_0^-$  for the  $z$  component. Then, to estimate the dominance of the greatest eigenvalue, we calculate the relative difference between  $\tau_{0,0}^+$  and the greatest between either of the secondary decay rates. Figs. 7a) and b) show the relative variation between said eigenvalues for two different evaporation rates:  $\tau_{ev} = 100 T_D$  in a) and  $\tau_{ev} = 1000 T_D$  in b). We can see that, for fast evaporation and large, asymmetric cylinders, our simplified expression Eq. (28) will not capture well the decay of correlations, as there are several dominant decay rates of similar size. On the contrary, for larger evaporation rates, regardless of the dimensions of the cylinder, our model Eq. (28) is faithful to the true dynamics, as can be readily observed also in Fig. 7c), where for a fixed height  $L = 5d$ , only at short evaporation times or large radius (and therefore highly asymmetric cylinder) does the second largest eigenvalue become important.

The similarity between the largest decay rate  $\tau_{0,0}^+$  and the surface to volume ratio is studied in Fig. 7d), where for a fixed height  $L = 5d$  we calculate the relative difference between  $\tau_{0,0}^+$  and its approximation in Eq. (28),  $V\tau_{ev}/Sd$ , as a function of the cylinder radius and the evaporation rate. We observe that it is only for fast evaporation of a highly asymmetric cylinder that the surface to volume ratio does not modulate adequately the decay of correlations.

#### Appendix D: Details for Fisher information calculations

The Fisher information is an objective measure of the maximum accuracy that an statistical estimator can achieve about a given parameter provided an experimental setting. According to the Cramér-Rao bound, the Fisher information lower bounds the minimum mean-squared-error that can be achieved for the target parameter estimator. For this reason, it can be used to compare the expected performance of two different experimental protocols with the same target parameter. Here, we detail the calculations that lead to the approximate Fisher information ratios shown in the main text. Particular details on the Fisher information for frequency estimation with a coherent signal can be found in [44, 52], while for the free diffusion case the calculations are detailed in [42, 45].

Our starting point is the probability to find the qubit on its upper (lower) state following some evolution time of an initial equal superposition state subjected to the noisy magnetic signal created by a distribution of diffusing nuclei. We assume a single target frequency  $\delta$ , for which the magnetic signal is described as  $B(t) = a(t) \cos(\delta t) + b(t) \sin(\delta t)$ ,

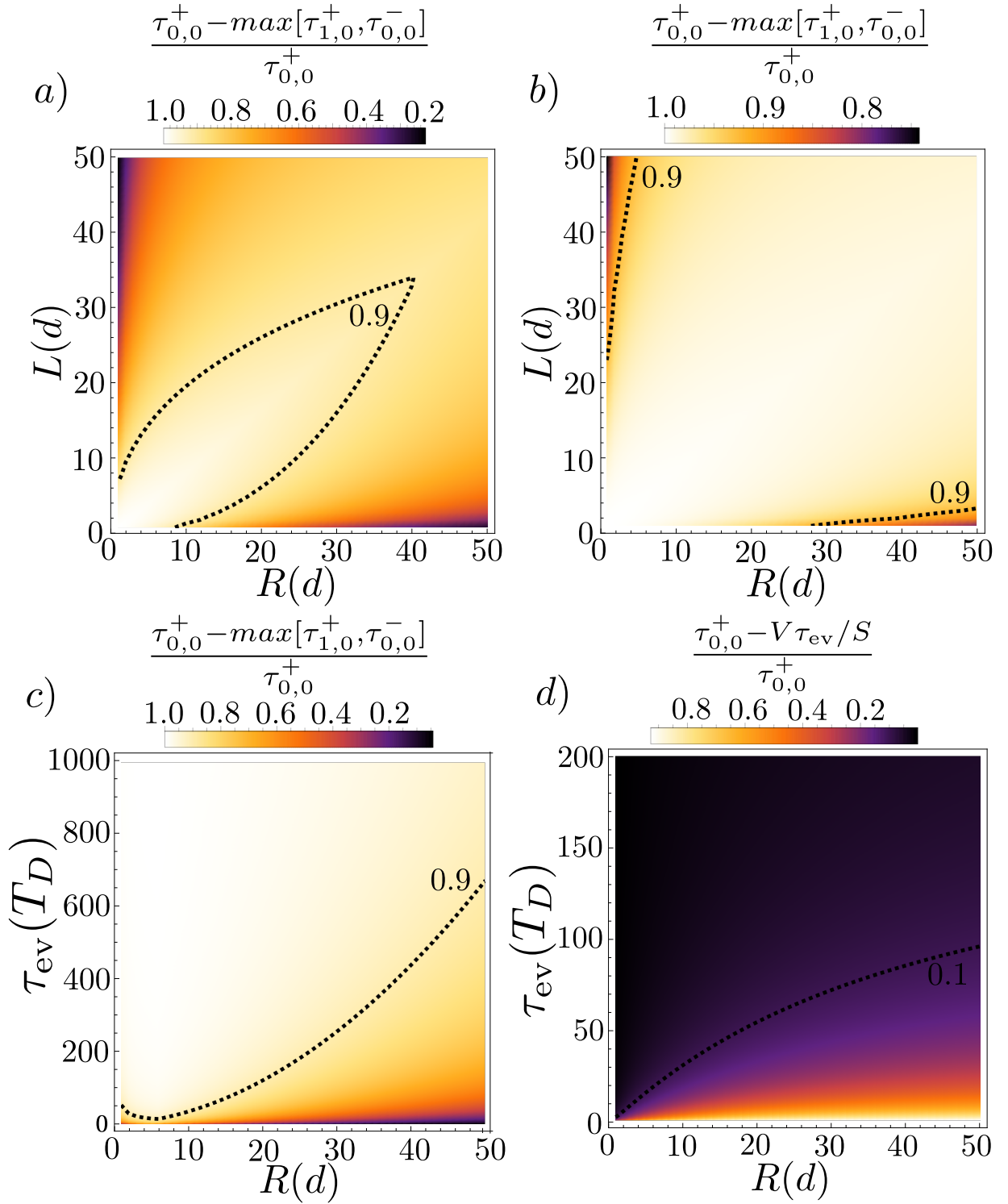


Figure 7. Relative variation between the greatest evaporation eigenvalue  $\tau_{0,0}$  with  $\eta_1^+$ , and the second greatest, which corresponds either to  $\tau_{1,0}$  with  $\eta_2^+$  or  $\tau_{0,0}$  with  $\eta_1^-$ , as a function of the cylinder size for two different evaporation times  $\tau_{ev} = 100T_D$  in a) and  $\tau_{ev} = 1000T_D$  in b), and as a function of the cylinder radius and  $\tau_{ev}$  for fixed height  $L = 5d$  in c). Relative variation between the greatest evaporation eigenvalue  $\tau_{0,0}$  and the ratio  $V\tau_{ev}/S$  in d) as a function of the cylinder radius and  $\tau_{ev}$  for fixed height  $L = 5d$ . In all cases, the dashed line marks the 10% relative change.

where the amplitudes  $\{a(t), b(t)\}$  follow some distribution due to noisy fluctuations. As a result of the interaction with the signal, the qubit probe acquires a phase that depends on  $B(t)$  and the particular dynamical decoupling sequence employed to control the qubit, which is modeled through the response function  $h(t)$ . This phase can be calculated as

$$\Phi[B(t')] = \gamma_n \int_{-\tau/2}^{\tau/2} ds h(s) B(t' + s), \quad (\text{D1})$$

with  $\tau$  the sequence duration and  $\gamma_n$  is the gyromagnetic ratio of the nuclei. If we assume that  $\tau$  is much smaller than any noise characteristic time affecting the system or the sample, and we consider that the pulses have negligible duration, the response function simplifies to  $h(t') = \theta(t' + \tau/2)\theta(t' - \tau/2)$ .

In Qdyne, after every phase acquisition period, an interrogation of the qubit state is performed. The probability to find the qubit in its upper state at that moment is  $P \propto \sin(\Phi_t)/2$ . The sequence of phase acquisition plus interrogation is repeated in a synchronised fashion throughout the experiment, keeping  $\tau$  constant, and controlling the interrogation and reinitialization time of the NV centre –the overhead time  $\tau_o$ – constant as well. Accurately tracking the time  $\tilde{\tau} = \tau + \tau_o$  enables reconstruction of the signal during the post-processing, and allows to correlate every pair of measurements, regardless of their temporal separation. Then, the relevant probability used to calculate the Fisher information is that of obtaining a pair of correlated measurements separated by an arbitrary time, which corresponds to the covariance between measurements. Assuming the weak signal limit this covariance reads  $\langle P_0 P_{j\tilde{\tau}} \rangle \sim \Phi_{\text{rms}}^2 \cos(\delta j \tilde{\tau}) G(j \tilde{\tau})$ , with  $j \in \mathbb{N}$  representing any given measurement. The Fisher information for one such correlated pair then reads  $i_\delta \propto \Phi_{\text{rms}}^4 t^2 \sin^2(\delta t) G^2(t)$ , and the total Fisher information  $I_\delta$  is the sum over all possible correlated pairs of measurements within the total experiment time. Considering that a single measurement has a duration  $\tilde{\tau}$ , we get that

$$I_\delta \propto \Phi_{\text{rms}}^4 \sum_{j=0}^{T/\tilde{\tau}} \left( \frac{T}{\tilde{\tau}} - j \right) (j \tilde{\tau})^2 \sin^2(\delta j \tilde{\tau}) [G(j \tilde{\tau})]^2, \quad (\text{D2})$$

where the extra factor  $(T/\tilde{\tau} - j)$  accounts for all possible subsequent measurements to which a given measurement can be correlated.

In the case of sticky walls, the distinct behaviour from free diffusion is achieved when the autocorrelation reaches the *plateau* section and stops decaying. At that point, the oscillating magnetic field behaves as a coherent signal with amplitude  $[G^{\text{sticky}}(t \gg \tau_V)]^2$ , meaning that the sum in Eq. (D2) can be calculated exactly as

$$I_\delta \propto [G^{\text{sticky}}(t \gg \tau_V)]^4 \sum_{j=0}^{T/\tilde{\tau}} \left( \frac{T}{\tilde{\tau}} - j \right) (j \tilde{\tau})^2 \sin^2(\delta j \tilde{\tau}) \approx \frac{[G^{\text{sticky}}(t \gg \tau_V)]^4 T_D T^3}{\tilde{\tau}^2}, \quad (\text{D3})$$

where we just keep the leading order in  $T$ , and assume that  $\delta T \gg 1$ . Thus we get Eq. (31) in the main text.

The case of evaporating walls is slightly more complicated, as the sum in Eq. (D2) cannot be calculated directly. Rather, we have to calculate it as an integral using the Riemann recipe. Additionally, rather than trying to calculate directly with the correlation function envelope Eq. (20), we use the various approximations depending on the different decay time-scales. Thus, for very fast evaporation  $\tau_{\text{ev}} \leq T_D$  we have that the correlations decay, approximately, as  $\sim t^{-3/2} \exp(-t/\tau_{\text{ev}})$ , and the Fisher information is

$$I_\delta^{\text{ev}} \sim \frac{\Phi_{\text{rms}}^4 T_D^4}{\tilde{\tau}^2} \int_0^{T/T_D} dz \left( \frac{T}{T_D} - z \right) z^2 \sin^2(\delta z T_D) \left[ z^{-3} \exp\left(-\frac{2z T_D}{\tau_{\text{ev}}}\right) \right], \quad (\text{D4})$$

where we use  $z = t/T_D$  for simplicity. Assuming that  $\delta T \gg 1$  and that  $\delta \tau_{\text{ev}} < 1$  this integral yields

$$I_\delta^{\text{ev}} \approx \frac{\Phi_{\text{rms}}^4 T_D^4 T}{8 \tilde{\tau}^2} \log(1 + \delta^2 \tau_{\text{ev}}^2 + \delta^4 \tau_{\text{ev}}^4), \quad (\text{D5})$$

with which we obtain Eq. (32) in the main text.

On the opposite end, when the evaporation time-scale is much longer than diffusion or the volume time  $\tau_{\text{ev}} \gg \{T_D, T_V\}$ , we can use the simplified model

$$G^{\text{ev}}(t) \approx B_{\text{rms}}^2 G^{\text{free}}(t/T_D) \exp(-2t/\tau_V) + G^{\text{ideal}}(t \gg \tau_V) \exp\left(-\frac{t}{\tilde{\tau}_{\text{ev}}}\right) \quad (\text{D6})$$



to calculate the Fisher information, where  $\tilde{\tau}_{\text{ev}} = V\tau_{\text{ev}}/Sd$ . Performing the the same sum to integral transformation as before we get that

$$\begin{aligned}
I_{\delta}^{\text{ev}} &\approx \frac{B_{\text{rms}}^4 T_D^4 \tau_V^3 \delta^2}{4\tilde{\tau}^2(T_D + T_D\tau_V^3\delta^2)} \\
&+ \frac{G^{\text{ideal}}(t \gg \tau_V)^4 \tilde{\tau}_{\text{ev}} T \left[ \tilde{\tau}_{\text{ev}}^2 - 2T^2 \exp\left(-\frac{2T}{\tilde{\tau}_{\text{ev}}}\right) \right]}{8\tilde{\tau}^2} \\
&+ \frac{G^{\text{ideal}}(t \gg \tau_V)^4 \tilde{\tau}_{\text{ev}} \left[ 3\tilde{\tau}_{\text{ev}}^3 - \exp\left(-\frac{2T}{\tilde{\tau}_{\text{ev}}}\right) (4T^3 + 6T^2\tilde{\tau}_{\text{ev}} + 6T\tilde{\tau}_{\text{ev}}^2 + 3\tilde{\tau}_{\text{ev}}^3) \right]}{16\tilde{\tau}^2} \\
&+ \frac{B_{\text{rms}}^2 G^{\text{ideal}}(t \gg \tau_V)^2 \tilde{\tau}_{\text{ev}} \tau_V}{4\sqrt{T_D}(\tilde{\tau}_{\text{ev}} + \tau_V)^2} \left\{ 2\sqrt{T} [3\tilde{\tau}_{\text{ev}}\tau_V + 2T(\tilde{\tau}_{\text{ev}} + \tau_V)] \exp\left(-\frac{T}{\tilde{\tau}_{\text{ev}}} - \frac{T}{\tau_V}\right) - 3\sqrt{\pi}\tilde{\tau}_{\text{ev}}\tau_V \sqrt{\frac{\tilde{\tau}_{\text{ev}}}{\tilde{\tau}_{\text{ev}} + \tau_V}} \right\} \\
&+ \frac{B_{\text{rms}}^2 G^{\text{ideal}}(t \gg \tau_V)^2 T \tilde{\tau}_{\text{ev}} \tau_V \sqrt{\pi}}{2\sqrt{T_D}(\tilde{\tau}_{\text{ev}} + \tau_V)} \sqrt{\frac{\tilde{\tau}_{\text{ev}}}{\tilde{\tau}_{\text{ev}} + \tau_V}} \\
&+ \frac{B_{\text{rms}}^2 T_D T}{8} \log(1 + 2\tilde{\tau}_{\text{ev}}\delta^2 + \tilde{\tau}_{\text{ev}}^4\delta^4). \tag{D7}
\end{aligned}$$

Considering the limit of large experiment time  $T \gg \tau_{\text{ev}}$ , as well as  $\delta T \gg 1$  and  $\delta\tau_{\text{ev}} < 1$  we get that the dominant term reads

$$I_{\delta}^{\text{ev}} \approx \frac{[G^{\text{ideal}}(t \gg \tau_V)]^4 \tilde{\tau}_{\text{ev}}^2}{16\tilde{\tau}^2} \left[ 2\tilde{\tau}_{\text{ev}}T + 2T^2 \exp\left(-\frac{2T}{\tilde{\tau}_{\text{ev}}}\right) \right] \tanh(\delta^2\tilde{\tau}_{\text{ev}}^2), \tag{D8}$$

which corresponds to Eq. (33) in the main text.